Specific amino acid substitutions in β strand S2 of FtsZ cause spiraling septation and impair assembly cooperativity in Streptomyces spp.

Sen, Beer Chakra; Wasserstrom, Sebastian; Findlay, Kim; Söderholm, Niklas; Sandblad, Linda; von Wachenfeldt, Claes; Flärdh, Klas

Published in:
Molecular Microbiology

DOI:
10.1111/mmi.14262

2019

Document Version:
Peer reviewed version (aka post-print)

Specific amino acid substitutions in β strand S2 of FtsZ cause spiraling septation and impair assembly cooperativity in *Streptomyces* spp.

Beer Chakra Sen[1], Sebastian Wasserstrom[1,#], Kim Findlay[2], Niklas Söderholm[3], Linda Sandblad[3], Claes von Wachenfeldt[1] and Klas Flärdh[1,*]

[1] *Department of Biology, Lund University, 223 62 Lund, Sweden*

[2] *Department of Cell & Molecular Biology, John Innes Centre, Norwich NR4 7UH, UK*

[3] *Department of Molecular Biology, Umeå University, 901 87 Umeå, Sweden.*

[#] *Present address:*

Lund University Bioimaging Center, 221 84 Lund, Sweden

**Corresponding author:*

Department of Biology, Lund University, Sölvegatan 35, 223 62 Lund, Sweden

Tel : (+46) 46 222 8584 Fax : (+46) 46 222 4113

Email : klas.flardh@biol.lu.se

Running Title: Twisted septation in *Streptomyces*

Keywords: cell division, cytoskeleton, cell wall, bacterial spores, *Streptomyces*

Summary

Bacterial cell division is orchestrated by the Z ring, which is formed by single-stranded treadmilling protofilaments of FtsZ. In *Streptomyces*, during sporulation, multiple Z rings are assembled and lead to formation of septa that divide a filamentous hyphal cell into tens of prespore compartments. We describe here mutant alleles of *ftsZ* in *Streptomyces coelicolor* and *Streptomyces venezuelae* that perturb cell division in such a way that constriction is initiated along irregular spiral-shaped paths rather than as regular septa perpendicular to the cell length axis. This conspicuous phenotype is caused by amino acid substitutions F37I and F37R in β strand S2 of FtsZ. The F37I mutation leads, instead of regular Z rings, to formation of relatively stable spiral-shaped FtsZ structures that are capable of initiating cell constriction. Further, we show that the F37 mutations affect the polymerization properties and impair the cooperativity of FtsZ assembly *in vitro*. The results suggest that specific residues in strand S2 of FtsZ affect the conformational switch in FtsZ that underlies assembly cooperativity and enable treadmilling of protofilaments, and that these features are required for formation of regular Z rings. However, the data also indicate FtsZ-directed cell constriction is not dependent on assembly cooperativity.

Introduction

Bacterial cell division is tightly regulated and coordinated with cell growth, replication, and segregation of the chromosome. The cytoskeletal protein FtsZ is the principle organizer of cell division in most bacteria and is also a focal point for the regulation of the process (for recent reviews, see Haeusser & Margolin, 2016, Ortiz *et al.*, 2016, Xiao & Goley, 2016). The assembly and function of the division machinery, also referred to as divisome, has been investigated in model organisms *Escherichia coli* and *Bacillus subtilis* (Du & Lutkenhaus, 2017, Errington & Wu, 2017). At first, FtsZ assembles as single protofilaments that coalesce into a ring-shaped pattern referred to as the Z ring. The precise localization of the Z ring at the mid-point of the cell is governed by regulatory proteins, such as Min proteins and DNA-associated nucleoid occlusion proteins (SlmA in *E. coli* and Noc in *B. subtilis*) (Rowlett & Margolin, 2015, Schumacher, 2017). Formation of the ring requires tethering of FtsZ to the membrane, which includes anchor-proteins such as FtsA and ZipA in *E. coli*, and FtsA and SepF in *B. subtilis* (Duman *et al.*, 2013, Pichoff & Lutkenhaus, 2005). Functionally redundant FtsZ-associated proteins, the Zaps (ZapA, ZapB, ZapC, and ZapD), also stabilize and promote the ring formation (Huang *et al.*, 2013, Ortiz *et al.*, 2016). All these components contribute to form the Z ring, which acts as a scaffold to recruit downstream core divisome proteins like FtsK, FtsQ, FtsL, FtsB, FtsW, FtsI and FtsN in a hierarchical manner, forming a 'mature divisome' (Aarsman *et al.*, 2005, Gamba *et al.*, 2009). Finally, the mature divisome coordinates cell wall synthesis to build a cross-wall of peptidoglycan at the site of division, invagination of other layers of the cell envelope, and eventually splitting of the cell.

The Z ring is a highly dynamic structure formed by individual and partially overlapping FtsZ protofilaments (reviewed in Erickson *et al.*, 2010, Haeusser & Margolin, 2016, Xiao & Goley, 2016). It has recently been shown that FtsZ protofilaments in the ring undergo rapid treadmilling activity that also drives the circumferential movement of the peptidoglycan (PG) synthesis machinery (Bisson-Filho *et al.*, 2017, Krupka & Margolin, 2018, Yang *et al.*, 2017). The treadmilling behaviour is coupled to GTPase activity and the GTP-driven cooperative assembly of FtsZ protofilaments (Yang *et al.*, 2017). *In vitro*, the treadmilling property is demonstrated by filaments undergoing dynamic reorganization as rotating vortices and is dependent on Mg^{2+} and FtsZ's GTPase activity (Loose & Mitchison, 2014, Ramirez-Diaz *et al.*, 2018). The cooperative polymerization is a prerequisite for treadmilling of single-stranded protofilaments. It is enabled by a conformational assembly switch in FtsZ structure between a

closed form (corresponding to a free monomer) and an open form (corresponding to the polymerized subunit) (Du *et al.*, 2018, Wagstaff *et al.*, 2017).

Actinobacteria, such as mycobacteria, corynebacteria, and streptomycetes, lack homologues of most proteins known to control Z-ring assembly in *E. coli* and other models, suggesting that they have different cell division control mechanisms that are not clearly known (McCormick, 2009). *Streptomyces* are filamentous, soil dwelling bacteria that have a complex developmental life cycle (Flärdh & Buttner, 2009, McCormick & Flärdh, 2012). In the vegetative mycelium, branching hyphae contain widely separated hyphal cross-walls. In response to nutrient depletion and other cues, specialized aerial hyphae emerge on the surface of colonies, become compartmentalized by multiple and developmentally regulated cell divisions, and differentiate eventually to chains of spores. The formation of these sporulation septa involves assembly of regularly placed Z rings in a ladder-like pattern along the length of the sporogenic hyphal cells (Grantcharova *et al.*, 2005, Schwedock *et al.*, 1997). Interestingly, the *ftsZ* gene (and cell division) is dispensable for vegetative growth but necessary for sporulation (McCormick *et al.*, 1994, Santos-Beneit *et al.*, 2017). Sporulation septation in *Streptomyces* involves also conserved core divisome proteins like FtsI, FtsQ, FtsW, FtsL, DivIC, FtsE, and FtsX (Jakimowicz & van Wezel, 2012, McCormick, 2009). However, none of the proteins involved in regulating Z-ring assembly or anchoring FtsZ to membrane in other groups of bacteria are conserved in *Streptomyces*, with the exception of SepF (Schlimpert *et al.*, 2017). The positioning of Z rings during spore formation have been reported to involve SsgA and SsgB, belonging to an actinomycete-specific family of proteins (Willemse *et al.*, 2011). Further, dynamin-like proteins DynA and DynB affect the stability and function of Z rings during sporulation (Schlimpert *et al.*, 2017), and a few additional genes, such as CrgA and SepG are reported that may directly affect the control cell division (Del Sol *et al.*, 2006, Zhang *et al.*, 2016). Overall, the mechanisms that control Z-ring formation and cell division in *Streptomyces* remain poorly understood.

In order to shed light on the developmentally controlled FtsZ assembly that occurs during sporulation in *Streptomyces*, we have used genetic strategies to identify mutations in *ftsZ* that affect sporulation septation (Grantcharova *et al.*, 2003, Wasserstrom *et al.*, 2013). Here, we describe an unusual type of *ftsZ* mutation that gives rise to spiral-shaped septa along the length of sporogenic hyphae, giving the hyphae a conspicuous twisted appearance. The mutations affect the region around α helix H1 and β strand S2 and perturb the assembly dynamics and shape of FtsZ polymers in the cell, but still allow initiation of cell constriction

even if proper Z rings have not formed. We also show that the mutations affect the critical concentration and cooperative assembly of FtsZ polymers, and thereby are likely to interfere with the treadmilling of FtsZ protofilaments.

Results

Identification of an ftsZ *mutant with spiralling sporulation septa*

Screens for *S. coelicolor* mutants specifically defective in sporulation have typically been based on the white colony phenotype (Whi) caused by absence of grey spore pigmentation (Chater, 1972, Hopwood *et al.*, 1970, Ryding *et al.*, 1999). A Whi phenotype is also caused by *ftsZ* mutations that affect developmentally controlled cell division in *S. coelicolor* (Flärdh *et al.*, 2000, Grantcharova *et al.*, 2003, Wasserstrom *et al.*, 2013). However, expression of late sporulation-specific genes, like those for spore pigment synthesis, may not be strictly dependent on multiple sporulation septation and occur also in some mutants with defective septation (see references and discussion in (Flärdh & Buttner, 2009)). Therefore, we devised a method to identify sporulation-defective *ftsZ* mutants that does not rely on the spore pigmentation and instead is based on replica plating. Wild-type S. *coelicolor* colonies produce large numbers of spores that readily transfer to new plates when replicated using velvet cloth. We speculated that mutants defective in sporulation septation would transfer less efficiently, and therefore screened a library of potential *ftsZ* mutants for strains that transfer poorly upon replica-plating of developed colonies from MS agar onto fresh plates. The library was constructed in an *ftsZ* null background harbouring an integrated plasmid with mutagenized *ftsZ* allele (See Experimental Procedures). One mutant that could be identified in this way has an unusual sporulation defect (see below), although it forms grey-pigmented colonies on MS agar plates that are very similar to the congenic *ftsZ*$^{+}$ strains like J2417 (Fig. 1).

The plasmid-borne *ftsZ* allele (termed *ftsZ28*) was extracted from the originally isolated mutant and confirmed to cause the observed septation defect by transfer back into a clean *ftsZ* null mutant strain. Microscopic examination of the aerial mycelium revealed that the mutant produces unusually shaped long aerial hyphal fragments instead of normal spore chains (Fig. 2). The fragments appear darker than regular hyphae in phase contrast microscopy, and are in that sense reminiscent of both wild-type spores and the spore-like hyphal fragments produced by some previously isolated *ftsZ* and *whiH* mutants (Flärdh *et al.*, 1999, Flärdh *et al.*, 2000, Grantcharova *et al.*, 2003). However, the hyphal fragments of this mutant also appear twisted

and show a very irregular cell contour, caused by invaginations or constrictions in the cell wall (Fig. 2B). The observations by phase contrast microscopy were supported by results from scanning electron microscopy, clearly revealing that the twisted appearance is due to helical or spiral-shaped constrictions running along many of the hyphae (Fig. 2D). Thin-sections of aerial mycelium from the mutant, examined by transmission electron microscopy, showed mostly irregular invaginations of the cell envelope and aberrantly shaped septations. A few apparently normal sporulation septa were seen (Fig. 2F), and some sporulation septa were completed and led to division, as evidenced by fragmentation of the irregularly shaped aerial hyphae (Fig. 2B).

The mutation in ftsZ28 *affects the same site on FtsZ as in two previously isolated mutants with spiralling septa in* E. coli *and* B. subtilis

Sequencing of the *ftsZ28* allele identified a single nucleotide substitution from T to A that results in change of a phenylalanine to an isoleucine residue at position 37 in *S. coelicolor* FtsZ. The affected residue is visualized in Fig. 3 in a structural model of *S. coelicolor* FtsZ that is based on a crystal structure of *Mycobacterium tuberculosis* FtsZ (Leung *et al.*, 2004, Wasserstrom *et al.*, 2013). Following the common nomenclature of secondary structure elements for tubulin and FtsZ proposed by Nogales *et al*. (Nogales *et al.*, 1998), the substitution occurs in the conserved β strand S2 in the N-terminal GTPase domain (Fig. 3A). F37 is conserved in the majority of bacterial FtsZs. For example, we found by sequence analysis using the protein families database, Pfam, that in FtsZ sequences from the phylum Actinobacteria it is either invariant (>99% out of 1180 sequences from 984 species) or replaced by tyrosine. The N-terminal domain of the structures of FtsZ from seven different bacteria and one archeon in different states (apo and nucleotide-bound states) all adopt essentially the same structure where the side chain corresponding to F37 (F, Y, L, or T) is buried into a hydrophobic region underneath α helix 1 (Fig. 3B and Fig. S1). Intriguingly, a survey of the literature shows that two mutations in this region of *ftsZ* in two different organisms have previously been reported to give rise to similar twisted septations (Fig. 3C). The *ftsZ26*(Ts) allele in *E. coli* causes abnormally shaped and often twisted septa at the permissive temperature, and this is caused by an insertion of six amino acids immediately adjacent to the phenylalanine that corresponds to F37 in *S. coelicolor* FtsZ (Addinall & Lutkenhaus, 1996, Bi & Lutkenhaus, 1992). Similar twisted division was observed in a large

fraction of cells carrying the allele *ftsZ20* in *Bacillus subtilis*, which causes the substitution of a highly conserved valine to alanine, corresponding to V35 in *S. coelicolor* FtsZ (Feucht & Errington, 2005).

F37 mutations in ftsZ *cause cell division defect in* S. venezuelae

Further investigations were carried out in the model organism *S. venezuelae* in order to take advantage of live cell imaging that is not possible in *S. coelicolor* (Schlimpert *et al.*, 2016). First, we determined whether mutations in other residues in the region around F37 would give rise to the unusual 'spiraling septation' phenotype. A series of mutations were introduced in *S. venezuelae ftsZ* on the ϕBT1 integrative plasmid pSS193 and transferred into the *ftsZ* deletion mutant DU500. Of the tested mutations, only F37I and one additional mutation, F37R, produced a 'spiraling septation' phenotype similar to the one observed in the *S. coelicolor* mutant (Table 1, Fig. 4B and D). The aerial hyphae of these mutants fail to complete sporulation septation and produce instead long twisted aerial hyphal fragments with spiral-shaped constrictions (Fig. 4B, F, D and H). Transmission electron microscopy revealed irregularly shaped constrictions and septa in these mutants compared to the regular septation in the wild type (Fig. S2). Mutations F37S, V35A, and V35D were tolerated in the sense that they allowed apparently normal sporulation septa to form. On the other hand, changing E36 or all three of G34-V35-E36 to alanines abolished sporulation septation completely. Finally, deletion of the three amino acid residues V35-E36-F37 gave an apparently detrimental allele that could not be introduced into the *ftsZ* null mutant strain (Table 1). These results suggest that only specific changes in the F37 residue give rise to the conspicuous spiraling septation phenotype.

In order to facilitate further analyses, the *ftsZ*(F37I) mutation was recombined onto the *S. venezuelae* chromosome to replace the native *ftsZ* allele (for details, see Experimental Procedures). Phase-contrast and scanning electron micrographs of this mutant (LUV056) confirmed that the sporulation defect and spiraling septation phenotype is similar to when the mutant *ftsZ* allele is placed on a plasmid in the Δ*ftsZ* mutant background in strain LUV050 (Fig. 4B, C, F and G).

Helical FtsZ assemblies in the ftsZ*(F37I) mutant*

To examine the effect of this mutation on the assembly and function of Z rings, we constructed strains with an FtsZ-YPet hybrid protein encoded by an integrative plasmid in the wild-type background and an FtsZ(F37I)-YPet hybrid in the *ftsZ*(F37I) background (strains LUV052 and LUV057, respectively). In both cases, the expression of these hybrid proteins is driven by native *ftsZ* promoters. Fluorescence imaging of hyphae from sporulating liquid cultures showed regular FtsZ ladders in the wild-type strain background, while helical cable-like FtsZ structures were observed in the *ftsZ*(F37I) mutant strain, indicating strong effects of the mutation on FtsZ assembly (Fig. 5A).

To better understand the effects of F37I mutation on the assembly and dynamics of FtsZ, we utilized microfluidics-based fluorescence live cell imaging (Schlimpert *et al.*, 2016). In the vegetative stage in the wild-type background, a typical single Z ring first appears to be dynamic and move along the hypha, before it becomes fixed at a certain position and increases in fluorescence intensity (Movie S1). Thereafter, the intensity of the ring gradually decreases, presumably while a cross wall is formed, although vegetative cross walls do not give rise to constrictions of hyphae and are not visible in the phase-contrast images. In the F37I mutant, fewer stable and bright Z rings, and mostly faint and apparently dynamic FtsZ structures are formed in the vegetative hypha compared to the wild type. Additionally, those rings that form appear to be tilted or mis-shaped (Movie S2), unlike in the wild type where they are placed perpendicular to the hyphal axis. In agreement with these observations, staining of cell walls in the *ftsZ*(F37I) mutant (LUV056) revealed that even though some regular hyphal cross-walls are formed, as in the wild type strain, most of the hyphal cross-walls are altered and seen as tilted or irregular structures (Fig. S3).

The most intriguing effect of the mutation is evident in sporulating hyphae, wherein *ftsZ* is upregulated and multiple Z rings start to assemble in order to form sporulation septa (Flärdh *et al.*, 2000, Kwak *et al.*, 2001). The developmental upregulation of *ftsZ* expression is visible as increasing overall fluorescence in specific hyphae in both wild type and mutant while these sporogenic hyphae are still extending (Movies S1 and S2). At the same time, FtsZ structures emerge but appear to dynamically change both positions and shape. The hyphae then stop growing in length, and around this time the Z rings in the wild type strain become fixed in position and show increased fluorescence intensity (Movie S1). A montage of a time series of a representative hypha with FtsZ-YPet is shown in Fig. 5B where time points are arranged in relation to the arrest of hyphal extension. Eventually, cell constriction, septum formation, and production of chains of equally sized spores are visible in the phase contrast images, and Z

rings disassemble (Movie S1 and Fig. 5B, top panel). The *ftsZ*(F37I) mutant shows a similar initial dynamic phase with faint FtsZ structures, but they become fixed as bright and stable spiral-shaped assemblies around the time of growth arrest (Movie S2, Fig. 5B, bottom panel, and Fig. S4). These mis-shaped spiral-like structures in the F37I mutant mostly remain unchanged over a long duration, suggesting stable structures and less dynamicity of the FtsZ polymers than with wild type FtsZ (Fig. 5B, bottom panel). Eventually, these coiled structures decrease gradually in fluorescence intensity and change shape, likely correlated with ingrowth of spiraling constrictions, although the constrictions are not clearly visible in the accompanying phase-contrast images. Constrictions and septa were instead stained and visualized using labeled wheat germ agglutinin in samples from sporulation cultures of the *ftsZ*(F37I) mutant (LUV056) in liquid medium. This revealed frequent aberrantly shaped patterns, including apparent spirals in the mutant, in comparison to regular arrangement of septa in the wild type (Fig. S5). Additionally, the mutant showed irregularly placed DNA within the sporulating hyphae, possibly suggesting issues in chromosome segregation (Fig. S5). In summary, the F37I mutation causes formation of helical FtsZ assemblies rather than regular Z rings in sporogenic hyphae, and these aberrant FtsZ structures are likely to direct formation of aberrantly shaped and often 'spiraling' septa (Fig. 4).

In vitro *analysis of mutant FtsZ*

In order to shed light on the biochemical basis of this unusual septation defect, we purified *S. venezuelae* wild-type FtsZ and the two mutant variants FtsZ(F37I) and FtsZ(F37R) and compared their GTPase activities. At our standard reaction conditions (pH 6.5, 30°C, 3.5 µM FtsZ, 50 µM GTP), the GTP hydrolysis rate of the FtsZ(F37I) mutant protein is lower, 0.40 ± 0.03 GTP per FtsZ per minute, compared to 0.79 ± 0.09 for the wild type FtsZ. The FtsZ(F37R) mutant variant has even lower GTP hydrolysis rate of 0.32 ± 0.03 (Fig. 6A). GTP-induced polymerization was further monitored using right-angle light scattering. Wild-type FtsZ quickly polymerizes upon GTP addition to reach a steady state level of polymerization/depolymerization, during which it hydrolyses the available GTP, followed by a decrease in polymerization revealed by a decline in light scattering (Fig. 6B). The F37 mutant proteins show an initial rise in polymerization upon GTP addition, where after the light scattering signals remain stable at a level lower than that of the wild type protein. The FtsZ(F37R) mutant variant showed the lowest light scattering signal among the tested

proteins, but the signal persisted for the longest time, which presumably is due to lower rate of GTP hydrolysis causing it to take longer time to deplete GTP in the reaction mixture. Observation of negatively stained FtsZ polymers by transmission electron microscopy revealed that the two mutant proteins mainly form protofilaments of shorter lengths than compared to the wild-type protein (Fig. 7), which could explain the lower light scattering signal seen for the mutant proteins. This trend was consistently seen in three different buffers with different pH (Fig. 7). The average length of polymers formed by wild type FtsZ was 177 ± 110, which is statistically significantly different from the polymers of mutant proteins that had lengths of 114 ± 58 nm for FtsZ(F37I) and 112 ± 58 nm for FtsZ(F37R) (Fig. S6).

Intriguingly, the FtsZ(F37I) mutant protein does not show a critical concentration (Cc) for GTPase activity. When comparing GTPase activities at different pH (pH 6.5; 6.9; 7.7), the largest difference in GTPase activity between wild type and mutant proteins was observed at pH 7.7 (Fig. S7). At this pH, the Cc of FtsZ wild-type protein was estimated to be 0.70 ± 0.01 μM, while the FtsZ(F37I) mutant protein does not show a Cc (Fig. 8). Also, under our standard conditions at pH 6.5 in MMK buffer, we saw what appeared to be isodesmic assembly with the mutant protein, contrasting to the wild-type protein that showed a Cc of 0.31 ± 0.02 μM (Fig. S8A). Since, the Cc is indicative of cooperativity, this result shows that the F37I mutation affects the cooperativity of FtsZ assembly. Assays of *S. coelicolor* FtsZ and its F37I mutant showed very similar results to those described above for the *S. venezuelae* proteins (Fig. S9). Similar to the *S. venezuelae* proteins, no critical concentration was observed for the *S. coelicolor* F37I mutant protein (Fig. S8B). In summary, the data show that the F37 mutations strongly affect the polymerization dynamics and interfere with the cooperativity of FtsZ assembly.

Discussion

One of the pieces of evidence that the FtsZ cytoskeleton defines the pattern of cell constriction and division in bacteria was provided by a mutant of *E. coli* in which mis-shaped twisted septa were correlated with similarly shaped FtsZ structures, organised as short helices rather than proper rings at the midpoint of the cell (Addinall & Lutkenhaus, 1996). However, many *ftsZ* mutations that perturb the shape of the Z ring into helices or other structures do not lead to correspondingly shaped constrictions (examples in (Grantcharova *et al.*, 2003, Michie *et al.*, 2006, Redick *et al.*, 2005, Stricker & Erickson, 2003)). The differences in effect on

septation are likely due to which stage of Z-ring formation that is affected by the mutations. It has been shown in several bacterial model systems that assembly of the cell division machinery is a multi-step process, including initial formation of the Z-ring aided by 'early' divisome proteins, followed after a time delay by maturation of the divisome and recruitment of 'late' division proteins (Aarsman *et al.*, 2005, Gamba *et al.*, 2009, Goley *et al.*, 2011, Tsukanov *et al.*, 2011). Thereafter initiation of cell constriction is triggered, which in *E. coli* involves the FtsN protein (Weiss, 2015), and finally the divisome is disassembled concomitantly with ingrowth and closure of the septum (Söderström *et al.*, 2016). The kind of *ftsZ* mutations described in this paper clearly perturb the early assembly and the shape of the cytokinetic FtsZ structures that are formed in the bacterium, but they are unusual in the sense that the mis-shaped polymers that are formed are still competent of directing constriction of the cell envelope, thereby leading to spiral-shaped or 'twisted' division furrows.

The mutations studied here affect a broadly conserved aspect of FtsZ function since very similar phenotypic effects are caused by mutations within a few amino acid residues of FtsZ in three distantly related types of bacteria: *E. coli* (Addinall & Lutkenhaus, 1996), *B. subtilis* (Feucht & Errington, 2005), and two species of *Streptomyces* (this paper). The three types of organisms use different proteins for control of the early stage of Z-ring assembly. FtsZ protofilaments in *E. coli* are anchored to the cell membrane by FtsA and ZipA, while *B. subtilis* uses FtsA and SepF (Du & Lutkenhaus, 2017, Errington & Wu, 2017). Streptomycetes lack FtsA, contain three orthologues of SepF, and in addition have been suggested to employ the SsgB protein for a positive control of Z-ring formation (Willemse *et al.*, 2011). Dynamins are also involved in the stabilization of Z rings during formation of sporulation septa in *Streptomyces* (Schlimpert *et al.*, 2017). In summary, mutations in or around a specific residue in β-strand 2 perturb Z-ring formation and affect a fundamental aspect of FtsZ function that is relevant irrespective of how Z-rings otherwise are regulated in the specific organism.

The mutations in F37 of *Streptomyces* FtsZ that lead to spiralling septation also changes the *in vitro* polymerization behaviour of FtsZ, reduces the GTPase activity, and appears to abolish the critical concentration for assembly. These findings should be interpreted in the light of the recent reports that treadmilling of FtsZ protofilaments is critical for the organization of the Z ring and for movement of the complexes of peptidoglycan synthesis enzymes during septum formation in *E. coli* and *B. subtilis* (Bisson-Filho *et al.*, 2017, Yang *et al.*, 2017). Interestingly, interference with cooperative assembly and GTPase activity of FtsZ, either by

sublethal concentrations of the FtsZ inhibitor PC190723 or specific mutations affecting GTPase activity, have been reported to perturb the shape of Z rings and also to cause 'twisted' and spiral-like cell constrictions (Adams *et al.*, 2011, Stokes *et al.*, 2013, Yang *et al.*, 2017). Benzamides, including compound PC190723, are known to bind to a specific site on the C-terminal activation domain of FtsZ that corresponds to the taxol binding site on tubulins, affect cooperativity, and cause stabilization of FtsZ polymers (Adams *et al.*, 2016, Andreu *et al.*, 2010, Elsen *et al.*, 2012, Haydon *et al.*, 2008). The reduced GTPase activity and lost cooperativity caused by our F37 mutations in *Streptomyces* are consistent with these findings, and we speculate that it leads to alteration of the treadmilling behaviour of FtsZ protofilaments, which in turn leads to formation of mis-shaped helical structures rather than proper Z rings. Adams *et al.* observed that benzamides induce a highly curved shape of *B. subtilis* FtsZ polymers *in vitro* and suggested that the abnormal divisions in benzamide-treated cells is related to FtsZ protomers adopting geometries that are incompatible with assembly into regular rings (Adams *et al.*, 2011). However, the protofilaments formed *in vitro* by the F37I or F37R mutant proteins did not show any significant curvature compared to the wild type FtsZ (Fig. 7). Thus, we find no evidence that the general shape of FtsZ protofilaments is perturbed by the F37 mutations, and it seems rather that the altered polymerization dynamics leads to assembly of helical structures in the cells.

Treadmilling of FtsZ protofilaments drives the circumferential motion of peptidoglycan synthesis complexes around the ingrowing septum in *E. coli* and *B. subtilis* (Bisson-Filho *et al.*, 2017, Yang *et al.*, 2017). If that is the case also in *Streptomyces*, it is not clear how these *ftsZ* mutations that interfere with GTPase activity and cooperative assembly of FtsZ could still allow deep septum-like division furrows to form in the F37 mutants. A possible explanation is provided by a recent report by Monteiro *et al.*, who found that constriction of Z rings in *Staphylococcus aureus* occurs in two stages, in which the assembly and initial constriction of the Z ring requires treadmilling, but the ring thereafter transitions to a second phase (involving the establishment of the peptidoglycan biosynthesis apparatus at the division site) where septum synthesis becomes independent of FtsZ treadmilling (Monteiro *et al.*, 2018). Extrapolating from this information, we suggest that the F37I and F37R mutations in *Streptomyces* interfere with the polymerization dynamics that underlie the assembly and initial constriction of the Z ring in such a way that proper rings are not formed, but recruitment of the apparatus for peptidoglycan assembly to the helical FtsZ structures is not

prevented, allowing transition to a stage in which septation is less sensitive to disturbed FtsZ dynamics, and leading to formation of helical septa and deep cell division furrows.

The F37 residue is far (>14 Å) from both the nucleotide binding pocket and the binding site of the inhibitor PC190723. So how do mutations in this residue affect GTPase activity? One possibility is that the mutations interfere with a conformational change required for cooperative assembly of FtsZ. In order to explain the basis for treadmilling behaviour of single-stranded protofilaments, an assembly switch has been proposed and evidence for such a switch have been reported in which FtsZ adopts two distinct conformations, an open form in filaments and a closed form in monomers (Wagstaff *et al.*, 2017). Interestingly, the switch involves opening of a hydrophobic cleft between α helix H7 and the C-terminal activation domain that constitutes the binding pocket for PC190723, and PC190723 appears to stabilize FtsZ in the open conformation, thereby stabilizing the polymeric form (Elsen *et al.*, 2012, Wagstaff *et al.*, 2017). It is an attractive idea that the F37 mutations could affect this assembly switch and thereby alter the ability of the protein to exhibit treadmilling. The residue in *S. aureus* FtsZ that corresponds to F37 is not directly affected by the proposed assembly switch, but nearby residues are indeed involved in the switch (Elsen *et al.*, 2012, Wagstaff *et al.*, 2017). The F37 mutations may communicate a structural change of the C-terminal domain via the interactions between helix H1 and helix H7.

Experimental Procedures

Strains, plasmids and growth conditions

Bacterial strains used in this study are listed in Table S1. The *S. venezuelae* strains are derivatives of strain NRRL B-65442 and *S. coelicolor* strains are derivatives of strain M145. *E. coli* strain DH5α was used for cloning and plasmid propagation. Other *E. coli* strains and plasmids are listed in Table S1 and S2, respectively. Growth conditions, antibiotic supplements, and genetic manipulation were as described previously for *E. coli* (Sambrook & Russel, 2001) and *Streptomyces* (Kieser *et al.*, 2000), unless otherwise stated. *S. venezuelae* strains were grown on maltose yeast extract medium (MYM) agar plates or in MYM liquid medium, as described by Bush *et al*. (Bush *et al.*, 2013). *S. coelicolor* strains were cultivated on mannitol soya flour (MS) agar plates or in yeast extract-malt extract (YEME) liquid medium (Kieser *et al.*, 2000).

404

405 *Strategy for isolation of* ftsZ *mutants defective in sporulation in* S. coelicolor

406 The generation of randomly mutagenized *S. coelicolor ftsZ* cloned in plasmid pKF32, and the
407 introduction of libraries into the *S. coelicolor ftsZ* null mutant HU133 was done as described
408 previously (Wasserstrom *et al.*, 2013). The plasmid can be transferred from *E. coli* to
409 *Streptomyces* by conjugation and integrates at the ϕC31 *attB* site on the *S. coelicolor*
410 chromosome. About 4000 exconjugants were patched on master MS agar plates containing 25
411 μg ml^{-1} apramycin, allowed to grow and sporulate, and each master plate was then replica
412 plated using a sterile velvet cloth on two nutrient agar (NA) plates, which were incubated at
413 30°C for 2 days. The density of growth in each patch on the NA plates, particularly the
414 second plate to be replicated from the same velvet, was used as an indicator of the efficiency
415 of sporulation, and strains that transferred poorly to the replicated plates were selected. Aerial
416 mycelia (on MS agar) from such candidate strains were examined by phase-contrast
417 microscopy to identify those with defects in sporulation septation. As described previously
418 (Wasserstrom *et al.*, 2013), the *ftsZ*-containing plasmid was recovered from such strains, and
419 transferred back to *S. coelicolor* strain HU133. The ex-conjugants that gave rise to colonies
420 with the same phenotype as the originally isolated strain were kept and the *ftsZ* allele on the
421 corresponding plasmids was sequenced. One *ftsZ* mutant allele that gave defective sporulation
422 but with a grey plate phenotype was designated as *ftsZ28* (strain K263), and the plasmid
423 carrying this allele was named pKF320.

424

425 *Construction of* ftsZ *mutants in* S. venezuelae *using integrative plasmid*

426 Using different primer pairs (Table S3) with phosphorylated 5'-ends, back-to-back PCR was
427 performed to generate various *ftsZ* mutations (the mutations are listed in Table 1) on plasmid
428 pSS193. PCR products were ligated and transformed into *E. coli* strain DH5α. The resulting
429 plasmids were verified by sequencing using primers KF1245 and KF1246 (See Table S2 for
430 list of primers). Plasmids were transformed into the promiscuous conjugation donor strain
431 ET12567/pUZ8002 and introduced by conjugation into an *S. venezuelae ftsZ* null mutant
432 (DU500), as described previously (Kieser *et al.*, 2000). Upon conjugation, plasmids integrate
433 at ϕBT1 *attB* site on *S. venezuelae* chromosome, resulting in strains listed in Table 1 and
434 Table S1. Ex-conjugants were purified on MYM agar plates containing nalidixic acid (25 μg
435 ml^{-1}) and hygromycin (50 μg ml^{-1}).

436

437 *Isolation of* ftsZ *chromosomal mutant*

438 To introduce point mutations into the native *ftsZ* locus on the *S. venezuelae* chromosome, a
439 plasmid vector marked with the β-glucuronidase gene *gusA* was used (Ladwig *et al.*, 2015,
440 Myronovskyi *et al.*, 2011) with a few modifications. *S. venezuelae ftsZ* with flanking DNA
441 was PCR amplified using primer pair KF1377/KF1378 and *S. venezuelae* genomic DNA as a
442 template. The PCR product was cloned into pUC18 at *Xba*I and *Eco*RI sites to yield plasmid
443 pKF550. The wild-type *ftsZ* gene in pKF550 was modified by exchanging a *Bst*XI-*Blp*I
444 fragment for the corresponding fragment from plasmid pKF534. The resulting plasmid
445 pKF606 contains *S. venezuelae ftsZ* with the F37I mutation and approximately 1500 flanking
446 base pairs on each side of the mutation. Using restriction sites for *Hind*III and *Eco*RI, this
447 insert with introduced mutation from pKF606 was cloned into pGus21, resulting in pKF608.
448 Correct plasmid construct was confirmed using restriction digestion with *Acl*I and *Sca*I and
449 sequencing with primers KF1245 and KF1266. The verified plasmid was transformed into *E.*
450 *coli* ET12567/pUZ8002 and introduced into *S. venezuelae* wild type by conjugation (as
451 described above). Ex-conjugants were transferred to and purified on MYM agar plates
452 containing nalidixic acid (25 μg ml^{-1}) and apramycin (50 μg ml^{-1}). Apramycin-resistant ex-
453 conjugants were selected that carried pKF608 integrated via single crossover. To screen for
454 second crossover resulting in *ftsZ*(F37I) mutation being retained on the chromosome, co-
455 integrants were plated for sporulation on MYM agar plates without antibiotics. Spores were
456 harvested and plated onto LB agar plates to obtain single colonies. After 1-2 days of
457 incubation at 30°C, plates were overlaid with 1 ml of deionized water containing 4.8 mM 5-
458 bromo-4-chloro-3-indolyl-β-D-glucuronic acid (X-GlcA; Duchefa Biochemie). Plates were
459 incubated further at 30°C to stain colonies that carry the integrated plasmid as observed by
460 blue halo due to X-GlcA hydrolysis by β-glucuronidase activity. White colonies, which are
461 the result of double crossover, were picked, purified, and tested for apramycin sensitivity on
462 MYM agar plates to confirm loss of plasmid. Correct mutant genotype was confirmed by
463 PCR analyses using primers KF1245/KF1277 and sequencing verification using primer
464 KF1266. A strain obtained with correct *ftsZ*(F37I) mutation was named LUV056.

465

466 *Fluorescent protein fusions*

An *ftsZ-ypet* fusion was amplified by PCR from pKF351 (Donczew *et al.*, 2016), using primer pair KF1290/KF1291, and the product was digested using *Avr*II and *Hind*III and cloned into pIJ10770. The resulting plasmid pKF543 was verified by DNA sequencing. Similarly, plasmid pKF540 was obtained by amplifying the *ftsZ*(F37I) allele from pKF534 using primer pair KF1273/KF1274 and ligating into the *Xba*I and *Nde*I sites on pKF351 to create a fusion to the *ypet* gene. Using plasmid pKF540, the fusion was PCR-amplified with primer pair KF1273/KF1291 and cloned into *Avr*II and *Hind*III site of pIJ10770. The resulting plasmid was named pKF544 and was verified by sequencing. Plasmids pKF543 and pKF544 were transformed into *E. coli* ET12567/pUZ8002. Conjugative transfer of the plasmids to *S. venezuelae* wild type and strain LUV056 was done as described above. Upon purification of colonies on selective MYM agar plates, strains LUV052 (*ftsZ*$^{+}$ *attB*$_{\phi BT1}$::pKF543[*ftsZ-ypet*]) and LUV057 (*ftsZ*(F37I) *attB*$_{\phi BT1}$::pKF544 [*ftsZ*(F37I)-*ypet*]) were obtained.

Microscopy

For phase-contrast microscopy of aerial hyphae and spores, colonies were allowed to grow and sporulate at 30°C on MYM or MS agar plates. Aerial hyphae and spores were sampled by pressing a cover slip against the colony surface and mounting on a slide coated with 1% agarose in phosphate buffered saline (PBS). In order to visualize hyphal-cross walls in vegetatively growing hyphae, cultures grown in MYM at 30°C and were stained with fluorescently labeled vancomycin as described previously (Grantcharova *et al.*, 2003). Cell wall and DNA staining of sporulating cultures with Wheat germ agglutinin-Oregon Green (Molecular Probes) and 7-Aminoactinomycin D (Molecular Probes) was done as described previously (Schwedock *et al.*, 1997). For visualizing fluorescent FtsZ-YPet fusion protein, cells were grown in liquid MYM and transferred to agarose-coated slides. To study FtsZ dynamics using the FtsZ-YPet fusion, time-lapse microscopy was performed using the CellASIC ONIX system and B04A-03 microfluidic plates (Merck Millipore), as described previously (Schlimpert *et al.*, 2016). Imaging was performed on a Zeiss AxioObserver.Z1 microscope with Illuminator HXP 120 V lamp (Zeiss) and Zeiss filter sets 46 HE YFP and 50 Cy5, Zeiss Plan-Apochromat 100×/1.4 Oil Ph3 objective, ZEN software (Zeiss) and an ORCA Flash 4.0 LT camera (Hamamatsu). Fiji (Schindelin *et al.*, 2012) was used to generate images (also from electron microscopy) and movies, as previously described (Schlimpert *et al.*, 2016).

To perform scanning electron microscopy, cells on the surface of developing colonies were plunged into liquid nitrogen slush and transferred to cryo preparation chamber (Gatan Alto 2500 or Quorum Technologies PP3000T) for sublimation at -90° to -95°C for 3 min and coated with thin layer of platinum. Imaging was performed with Supra 55 VP or Merlin field-emission scanning electron microscopes (Carl Zeiss Ltd, Germany) using in-chamber secondary electron detector at accelerating voltage of 1.2 to 5.0 kV and probe currents of 50-100 pA. To perform transmission electron microscopy of aerial hyphae and spores, colonies were fixed in 2.5% (vol/vol) glutaraldehyde in 0.1 M sodium cacodylate buffer, stained with 1% osmic acid, dehydrated in graded series of ethanol and embedded in LR White resin according to the manufacturer's instructions (The London Resin Co.). 70 nm sections were cut on a UCF 7 ultramicrotome (Leica Microsystems (UK) Ltd, Milton Keynes), contrasted with Uranyl acetate (5%) and Pb-citrate (0.1%) and imaged in a FEI Talos L120C transmission electron microscope with FEI CETA detector.

Heterologous FtsZ protein production in E. coli

Production and purification of FtsZ proteins were done using IMPACT system (New England Biolabs) as described previously (Wasserstrom *et al.*, 2013), unless otherwise stated. PCR amplification of *S. venezuelae ftsZ* without stop codon was done using primers KF44/KF1277 and template plasmid pSS193. The primer KF44 contains an *Nde*I restriction site and thus the PCR product on digestion with *Nde*I restriction enzyme generates a fragment with a sticky 5' end and a blunt 3' end. This fragment was ligated into *Nde*I and *Sma*I site in expression plasmid pTYB2. The resulting plasmid pKF541 was used for production of *S. venezuelae* FtsZ fused at its C-terminus to intein-chitin-binding domain (CBD) of the IMPACT system. Induction of intein self-cleavage releases *S. venezuelae* FtsZ with one additional glycine residue at the C-terminus. For the expression and production of FtsZ(F37I) and FtsZ(F37R), plasmids pKF542 and pKF546 were constructed in the same way as pKF541, but starting from template plasmids pKF534 and pKF530, respectively. *S. coelicolor* FtsZ was produced with plasmid pKF176. Site-directed mutagenesis to introduce the *ftsZ28* mutation F37I into *S. coelicolor ftsZ* was done as described previously, using primer pair KF879/KF880 (Wasserstrom *et al.*, 2013). The resulting plasmid was named pKF328. Protein production, affinity purification, and induction of intein self-cleavage was done as described previously (Wasserstrom *et al.*, 2013). Each dialyzed sample was further subjected to size exclusion

chromatography on a 320 ml HiLoad 26/600 Superdex 75 pg gel filtration column (GE Healthcare) connected to an ÄKTA Purifier system (GE Healthcare) using SEC buffer (20 mM HEPES-KOH, 50 mM KCl, 0.1 mM EDTA, 10 % v/v glycerol, pH 7.2) and run at 2 ml min^{-1} at 8°C. Peak fractions were analysed on Criterion TGX Any kD precast SDS-PAGE gels (BioRad), and appropriate fractions were pooled and concentrated using Millipore Amicon ultrafiltration spin columns (MWCO 10,000). The protein concentration of wild-type FtsZ (both *S. coelicolor* and *S. venezuelae*) was determined by quantitative amino acid analysis (Alphalyse, Denmark) and used as a reference to validate concentrations measured using DC Protein Assay kit II (Bio-Rad). Protein preparations were aliquoted, snap frozen using liquid N_2, and stored at -80°C in SEC buffer.

In vitro *analysis of FtsZ proteins*

The Malachite Green-based assay to determine GTPase activity (PiColorLock Gold, Expedeon) and right-angle light scattering to monitor polymerization activity were performed as described previously (Wasserstrom *et al.*, 2013), unless otherwise stated. GTPase activities were determined from the linear range of GTP hydrolysis reaction curves. For critical concentration (Cc) determination, GTPase assays were performed as described previously (Krol & Scheffers, 2013), with some modifications. The reactions were performed at 30°C, wherein FtsZ concentrations 0.75, 1.25, 1.75, 2.25, and 2.75 µM were used with 500 µM GTP in either MMK buffer (50 mM MES-KOH, 10 mM MgAc, 200 mM KAc, pH 6.5) or HMK buffer (50 mM HEPES-KOH, 5 mM MgAc, 200 mM KAc, pH 7.7). Negative staining transmission electron microscopy was used to visualize FtsZ protofilaments. 3.5 µM of FtsZ (5 variants) was polymerized at 30°C in buffers with 500 µM GTP. Buffers used for this assembly were 50 mM MES (pH 6.5) or 50 mM MOPS (pH 6.9) or 50 mM HEPES (pH 7.7), each containing 200 mM KAc and 10 mM MgAc. Samples were diluted 10-fold in the same buffers before, and 3.5 µl of the samples were spotted on carbon-coated copper grids and incubated for 1 min at 30°C. The grids were then quickly washed twice in 50 µl drops of deionized water, followed by one quick dipping in a 50 µl drop of 1.5% uranyl acetate and 30 sec in a second drop of uranyl acetate. Grids were then carefully blotted against Whatman filter paper. Stained specimens were air dried and imaged with JEOL JEM-1230 electron microscope at 80,000x magnification. Images were acquired with Gatan Orius CCD camera.

Bioinformatic analysis

Bacterial FtsZ sequences were collected from the Pfam database (El-Gebali *et al.*, 2019) (family PF00091) and aligned using Kalign (Lassmann & Sonnhammer, 2005). Sequence alignment of FtsZ with known structures was done using T-COFFEE (Di Tommaso *et al.*, 2011) and annotated using ESPript (Robert & Gouet, 2014). Graphical representations of three-dimensional models of FtsZ were prepared by using PyMOL (The PyMOL Molecular Graphics System, Schrödinger, LLC).

Acknowledgements

We thank Fanny Passot and Markus Fröjd for technical assistance; Susan Schlimpert and Günther Muth for gifts of plasmids; Joel Hallgren and Ted Lindström for help with protein biochemistry; Lund Protein Production Platform (LP3) for help with large-scale protein purification; the National Microscopy Infrastructure, NMI (VR-RFI 2016-00968) at Umeå Core facility for Electron Microscopy, UCEM, Umeå University, and the Bioimaging core facility at the John Innes Centre, Norwich, funded by BBSRC, for assistance with SEM and TEM; Ala Javadi, Cheng Choo Lee, Gayathri Vegesna, Maria Baumgarten and Rita Wallén for excellent technical assistance with electron microscopy. Support from the Sven och Lilly Lawskis fond för naturvetenskaplig forskning (BCS); Swedish Research Council Grants 621-2007-4767 and 621-2010-4463 (KlF); the Crafoord Foundation (KlF); and a PhD studentship within the Research School in Pharmaceutical Sciences at Lund University (SW).

Data availability statement

The data that support the findings of this study are available from the corresponding author upon reasonable request.

Conflict of Interest

The authors declare that they have no conflicts of interest with the contents of this article.

Author contributions

KlF conceptualized the study and obtained funding. BCS, SW and KlF designed experiments, analyzed data and prepared original draft of the manuscript. SW performed initial experiments on *S. coelicolor*, BS carried out most of the experiments including biochemical

assays of *S. coelicolor* proteins, while KiF, NS and LS performed electron microscopy experiments. CvW analyzed data in relation to available FtsZ structures. BCS, SW, and KlF wrote the paper with input from all authors.

Graphical abstract

Abbreviated Summary

Mutations were identified in *ftsZ* that give rise to spiraling cell constrictions instead of the regularly spaced septa that normally convert hyphae to spores in *Streptomyces* spp. The mutations affect a conserved region of FtsZ (β strand S2 and α helix H1), cause FtsZ to assemble into helical structures in the cell, and abolish the cooperativity in polymerization assays *in vitro*. The data suggest that this region of FtsZ is critical for cooperative assembly and proper Z-ring formation, probably by affecting treadmilling, and further indicate that these features are not required for cell constriction.

References

Aarsman, M.E., Piette, A., Fraipont, C., Vinkenvleugel, T.M., Nguyen-Disteche, M., and den Blaauwen, T. (2005) Maturation of the *Escherichia coli* divisome occurs in two steps. *Mol. Microbiol.* **55**: 1631-1645.

Adams, D.W., Wu, L.J., Czaplewski, L.G., and Errington, J. (2011) Multiple effects of benzamide antibiotics on FtsZ function. *Mol. Microbiol.* **80**: 68-84.

Adams, D.W., Wu, L.J., and Errington, J. (2016) A benzamide-dependent *ftsZ* mutant reveals residues crucial for Z-ring assembly. *Mol. Microbiol.* **99**: 1028-1042.

Addinall, S.G., and Lutkenhaus, J. (1996) FtsZ-spirals and -arcs determine the shape of the invaginating septa in some mutants of *Escherichia coli*. *Mol. Microbiol.* **22**: 231-237.

Andreu, J.M., Schaffner-Barbero, C., Huecas, S., Alonso, D., Lopez-Rodriguez, M.L., Ruiz-Avila, L.B., Nunez-Ramirez, R., Llorca, O., and Martin-Galiano, A.J. (2010) The antibacterial cell division inhibitor PC190723 is an FtsZ polymer-stabilizing agent that induces filament assembly and condensation. *J. Biol. Chem.* **285**: 14239-14246.

Bi, E., and Lutkenhaus, J. (1992) Isolation and characterization of *ftsZ* alleles that affect septal morphology. *J. Bacteriol.* **174**: 5414-5423.

Bisson-Filho, A.W., Hsu, Y.P., Squyres, G.R., Kuru, E., Wu, F., Jukes, C., Sun, Y., Dekker, C., Holden, S., VanNieuwenhze, M.S., Brun, Y.V., and Garner, E.C. (2017) Treadmilling by FtsZ filaments drives peptidoglycan synthesis and bacterial cell division. *Science* **355**: 739-743.

Bush, M.J., Bibb, M.J., Chandra, G., Findlay, K.C., and Buttner, M.J. (2013) Genes required for aerial growth, cell division, and chromosome segregation are targets of WhiA before sporulation in *Streptomyces venezuelae*. *MBio* **4**: e00684-00613.

Chater, K.F. (1972) A morphological and genetic mapping study of white colony mutants of *Streptomyces coelicolor* A3(2). *J. Gen. Microbiol.* **72**: 9-28.

Del Sol, R., Mullins, J.G., Grantcharova, N., Flärdh, K., and Dyson, P. (2006) Influence of CrgA on assembly of the cell division protein FtsZ during development of *Streptomyces coelicolor*. *J. Bacteriol.* **188**: 1540-1550.

Di Tommaso, P., Moretti, S., Xenarios, I., Orobitg, M., Montanyola, A., Chang, J.M., Taly, J.F., and Notredame, C. (2011) T-Coffee: a web server for the multiple sequence

alignment of protein and RNA sequences using structural information and homology extension. *Nucleic Acids Res.* **39**: W13-17.

Donczew, M., Mackiewicz, P., Wrobel, A., Flärdh, K., Zakrzewska-Czerwinska, J., and Jakimowicz, D. (2016) ParA and ParB coordinate chromosome segregation with cell elongation and division during *Streptomyces* sporulation. *Open Biol* **6**: 150263.

Du, S., and Lutkenhaus, J. (2017) Assembly and activation of the *Escherichia coli* divisome. *Mol. Microbiol.* **105**: 177-187.

Du, S., Pichoff, S., Kruse, K., and Lutkenhaus, J. (2018) FtsZ filaments have the opposite kinetic polarity of microtubules. *Proc. Natl. Acad. Sci. USA* **115**: 10768-10773.

Duman, R., Ishikawa, S., Celik, I., Strahl, H., Ogasawara, N., Troc, P., Löwe, J., and Hamoen, L.W. (2013) Structural and genetic analyses reveal the protein SepF as a new membrane anchor for the Z ring. *Proc. Natl. Acad. Sci. USA* **110**: E4601-E4610.

El-Gebali, S., Mistry, J., Bateman, A., Eddy, S.R., Luciani, A., Potter, S.C., Qureshi, M., Richardson, L.J., Salazar, G.A., Smart, A., Sonnhammer, E.L.L., Hirsh, L., Paladin, L., Piovesan, D., Tosatto, S.C.E., and Finn, R.D. (2019) The Pfam protein families database in 2019. *Nucleic Acids Res.* **47**: D427-D432.

Elsen, N.L., Lu, J., Parthasarathy, G., Reid, J.C., Sharma, S., Soisson, S.M., and Lumb, K.J. (2012) Mechanism of action of the cell-division inhibitor PC190723: modulation of FtsZ assembly cooperativity. *J. Am. Chem. Soc.* **134**: 12342-12345.

Erickson, H.P., Anderson, D.E., and Osawa, M. (2010) FtsZ in bacterial cytokinesis: cytoskeleton and force generator all in one. *Microbiol. Mol. Biol. Rev.* **74**: 504-528.

Errington, J., and Wu, L.J. (2017) Cell cycle machinery in *Bacillus subtilis*. *Subcell. Biochem.* **84**: 67-101.

Feucht, A., and Errington, J. (2005) *ftsZ* mutations affecting cell division frequency, placement and morphology in *Bacillus subtilis*. *Microbiology* **151**: 2053-2064.

Flärdh, K., and Buttner, M.J. (2009) *Streptomyces* morphogenetics: Dissecting differentiation in a filamentous bacterium. *Nat. Rev. Microbiol.* **7**: 36-49.

Flärdh, K., Findlay, K.C., and Chater, K.F. (1999) Association of early sporulation genes with suggested developmental decision points in *Streptomyces coelicolor* A3(2). *Microbiology* **145**: 2229-2243.

669 Flärdh, K., Leibovitz, E., Buttner, M.J., and Chater, K.F. (2000) Generation of a non-
670 sporulating strain of *Streptomyces coelicolor* A3(2) by the manipulation of a
671 developmentally controlled *ftsZ* promoter. *Mol. Microbiol.* **38**: 737-749.

672 Gamba, P., Veening, J.W., Saunders, N.J., Hamoen, L.W., and Daniel, R.A. (2009) Two-
673 step assembly dynamics of the *Bacillus subtilis* divisome. *J. Bacteriol.* **191**: 4186-4194.

674 Goley, E.D., Yeh, Y.C., Hong, S.H., Fero, M.J., Abeliuk, E., McAdams, H.H., and
675 Shapiro, L. (2011) Assembly of the *Caulobacter* cell division machine. *Mol. Microbiol.*
676 **80**: 1680-1698.

677 Grantcharova, N., Lustig, U., and Flärdh, K. (2005) Dynamics of FtsZ assembly during
678 sporulation in *Streptomyces coelicolor* A3(2). *J. Bacteriol.* **187**: 3227-3237.

679 Grantcharova, N., Ubhayasekera, W., Mowbray, S.L., McCormick, J.R., and Flärdh, K.
680 (2003) A missense mutation in *ftsZ* differentially affects vegetative and developmentally
681 controlled cell division in *Streptomyces coelicolor* A3(2). *Mol Microbiol* **47**: 645-656.

682 Haeusser, D.P., and Margolin, W. (2016) Splitsville: structural and functional insights into
683 the dynamic bacterial Z ring. *Nat. Rev. Microbiol.* **14**: 305-319.

684 Haydon, D.J., Stokes, N.R., Ure, R., Galbraith, G., Bennett, J.M., Brown, D.R., Baker,
685 P.J., Barynin, V.V., Rice, D.W., Sedelnikova, S.E., Heal, J.R., Sheridan, J.M., Aiwale,
686 S.T., Chauhan, P.K., Srivastava, A., Taneja, A., Collins, I., Errington, J., and Czaplewski,
687 L.G. (2008) An inhibitor of FtsZ with potent and selective anti-staphylococcal activity.
688 *Science* **321**: 1673-1675.

689 Hopwood, D.A., Wildermuth, H., and Palmer, H.M. (1970) Mutants of *Streptomyces*
690 *coelicolor* defective in sporulation. *J. Gen. Microbiol.* **61**: 397-408.

691 Huang, K.H., Durand-Heredia, J., and Janakiraman, A. (2013) FtsZ-ring stability: of
692 bundles, tubules, crosslinks and curves. *J. Bacteriol.* **195**: 1859-1868.

693 Jakimowicz, D., and van Wezel, G.P. (2012) Cell division and DNA segregation in
694 *Streptomyces*: how to build a septum in the middle of nowhere? *Mol. Microbiol.* **85**: 393-
695 404.

696 Kieser, T., Bibb, M.J., Buttner, M.J., Chater, K.F., and Hopwood, D.A., (2000) *Practical*
697 *Streptomyces Genetics*. The John Innes Foundation, Norwich, UK.

Krol, E., and Scheffers, D.J. (2013) FtsZ polymerization assays: simple protocols and considerations. *J. Vis. Exp.*: e50844.

Krupka, M., and Margolin, W. (2018) Unite to divide: Oligomerization of tubulin and actin homologs regulates initiation of bacterial cell division. *F1000Res* **7**: 235.

Kwak, J., Dharmatilake, A.J., Jiang, H., and Kendrick, K.E. (2001) Differential regulation of *ftsZ* transcription during septation of *Streptomyces griseus*. *J. Bacteriol.* **183**: 5092-5101.

Ladwig, N., Franz-Wachtel, M., Hezel, F., Soufi, B., Macek, B., Wohlleben, W., and Muth, G. (2015) Control of Morphological Differentiation of *Streptomyces coelicolor* A3(2) by Phosphorylation of MreC and PBP2. *PLoS One* **10**: e0125425.

Lassmann, T., and Sonnhammer, E.L. (2005) Kalign--an accurate and fast multiple sequence alignment algorithm. *BMC bioinformatics* **6**: 298.

Leung, A.K., Lucile White, E., Ross, L.J., Reynolds, R.C., DeVito, J.A., and Borhani, D.W. (2004) Structure of *Mycobacterium tuberculosis* FtsZ reveals unexpected, G protein-like conformational switches. *J. Mol. Biol.* **342**: 953-970.

Loose, M., and Mitchison, T.J. (2014) The bacterial cell division proteins FtsA and FtsZ self-organize into dynamic cytoskeletal patterns. *Nat. Cell Biol.* **16**: 38-46.

McCormick, J.R. (2009) Cell division is dispensable but not irrelevant in *Streptomyces*. *Curr. Opin. Microbiol.* **12**: 689-698.

McCormick, J.R., and Flärdh, K. (2012) Signals and regulators that govern *Streptomyces* development. *FEMS Microbiol. Rev.* **36**: 206-231.

McCormick, J.R., Su, E.P., Driks, A., and Losick, R. (1994) Growth and viability of *Streptomyces coelicolor* mutant for the cell division gene *ftsZ*. *Mol. Microbiol.* **14**: 243-254.

Michie, K.A., Monahan, L.G., Beech, P.L., and Harry, E.J. (2006) Trapping of a spiral-like intermediate of the bacterial cytokinetic protein FtsZ. *J. Bacteriol.* **188**: 1680-1690.

Monteiro, J.M., Pereira, A.R., Reichmann, N.T., Saraiva, B.M., Fernandes, P.B., Veiga, H., Tavares, A.C., Santos, M., Ferreira, M.T., Macario, V., VanNieuwenhze, M.S., Filipe, S.R., and Pinho, M.G. (2018) Peptidoglycan synthesis drives an FtsZ-treadmilling-independent step of cytokinesis. *Nature* **554**: 528-532.

728 Myronovskyi, M., Welle, E., Fedorenko, V., and Luzhetskyy, A. (2011) Beta-
729 glucuronidase as a sensitive and versatile reporter in actinomycetes. *Appl. Environ.*
730 *Microbiol.* **77**: 5370-5383.

731 Nogales, E., Downing, K.H., Amos, L.A., and Löwe, J. (1998) Tubulin and FtsZ form a
732 distinct family of GTPases. *Nat. Struct. Biol.* **5**: 451-458.

733 Ortiz, C., Natale, P., Cueto, L., and Vicente, M. (2016) The keepers of the ring: regulators
734 of FtsZ assembly. *FEMS Microbiol. Rev.* **40**: 57-67.

735 Pichoff, S., and Lutkenhaus, J. (2005) Tethering the Z ring to the membrane through a
736 conserved membrane targeting sequence in FtsA. *Mol. Microbiol.* **55**: 1722-1734.

737 Ramirez-Diaz, D.A., Garcia-Soriano, D.A., Raso, A., Mucksch, J., Feingold, M., Rivas,
738 G., and Schwille, P. (2018) Treadmilling analysis reveals new insights into dynamic FtsZ
739 ring architecture. *PLoS Biol.* **16**: e2004845.

740 Redick, S.D., Stricker, J., Briscoe, G., and Erickson, H.P. (2005) Mutants of FtsZ
741 targeting the protofilament interface: effects on cell division and GTPase activity. *J.*
742 *Bacteriol.* **187**: 2727-2736.

743 Robert, X., and Gouet, P. (2014) Deciphering key features in protein structures with the
744 new ENDscript server. *Nucleic Acids Res.* **42**: W320-324.

745 Rowlett, V.W., and Margolin, W. (2015) The Min system and other nucleoid-independent
746 regulators of Z ring positioning. *Front. Microbiol.* **6**: 478.

747 Ryding, N.J., Bibb, M.J., Molle, V., Findlay, K.C., Chater, K.F., and Buttner, M.J. (1999)
748 New sporulation loci in *Streptomyces coelicolor* A3(2). *J. Bacteriol.* **181**: 5419-5425.

749 Sambrook, J., and Russel, D.W., (2001) *Molecular Cloning: A Laboratory Manual*. Cold
750 Spring Harbor Laboratory Press, Cold Spring Harbor, NY.

751 Santos-Beneit, F., Roberts, D.M., Cantlay, S., McCormick, J.R., and Errington, J. (2017)
752 A mechanism for FtsZ-independent proliferation in *Streptomyces*. *Nat. Commun.* **8**: 1378.

753 Schindelin, J., Arganda-Carreras, I., Frise, E., Kaynig, V., Longair, M., Pietzsch, T.,
754 Preibisch, S., Rueden, C., Saalfeld, S., Schmid, B., Tinevez, J.Y., White, D.J.,
755 Hartenstein, V., Eliceiri, K., Tomancak, P., and Cardona, A. (2012) Fiji: an open-source
756 platform for biological-image analysis. *Nat. Methods* **9**: 676-682.

Schlimpert, S., Flärdh, K., and Buttner, M. (2016) Fluorescence time-lapse imaging of the complete *S. venezuelae* life cycle using a microfluidic device. *J. Vis. Exp.*: e53863.

Schlimpert, S., Wasserstrom, S., Chandra, G., Bibb, M.J., Findlay, K.C., Flärdh, K., and Buttner, M.J. (2017) Two dynamin-like proteins stabilize FtsZ rings during *Streptomyces* sporulation. *Proc. Natl. Acad. Sci. USA* **114**: E6176-E6183.

Schumacher, M.A. (2017) Bacterial nucleoid occlusion: multiple mechanisms for preventing chromosome bisection during cell division. *Subcell. Biochem.* **84**: 267-298.

Schwedock, J., McCormick, J.R., Angert, E.A., Nodwell, J.R., and Losick, R. (1997) Assembly of the cell division protein FtsZ into ladder-like structures in the aerial hyphae of *Streptomyces coelicolor*. *Mol. Microbiol.* **25**: 847-858.

Stokes, N.R., Baker, N., Bennett, J.M., Berry, J., Collins, I., Czaplewski, L.G., Logan, A., Macdonald, R., Macleod, L., Peasley, H., Mitchell, J.P., Nayal, N., Yadav, A., Srivastava, A., and Haydon, D.J. (2013) An improved small-molecule inhibitor of FtsZ with superior in vitro potency, drug-like properties, and in vivo efficacy. *Antimicrob. Agents Chemother.* **57**: 317-325.

Stricker, J., and Erickson, H.P. (2003) In vivo characterization of *Escherichia coli ftsZ* mutants: effects on Z-ring structure and function. *J. Bacteriol.* **185**: 4796-4805.

Söderström, B., Mirzadeh, K., Toddo, S., von Heijne, G., Skoglund, U., and Daley, D.O. (2016) Coordinated disassembly of the divisome complex in *Escherichia coli*. *Mol. Microbiol.* **101**: 425-438.

Tsukanov, R., Reshes, G., Carmon, G., Fischer-Friedrich, E., Gov, N.S., Fishov, I., and Feingold, M. (2011) Timing of Z-ring localization in *Escherichia coli*. *Phys. Biol.* **8**: 066003.

Wagstaff, J.M., Tsim, M., Oliva, M.A., Garcia-Sanchez, A., Kureisaite-Ciziene, D., Andreu, J.M., and Löwe, J. (2017) A polymerization-associated structural switch in FtsZ that enables treadmilling of model filaments. *MBio* **8**: e00254-00217.

Wasserstrom, S., Grantcharova, N., Ubhayasekera, W., Ausmees, N., Sandblad, L., and Flärdh, K. (2013) Non-sporulating *ftsZ* mutants in *Streptomyces coelicolor* reveal amino acid residues critical for FtsZ polymerization dynamics. *Microbiology* **159**: 890-901.

Weiss, D.S. (2015) Last but not least: new insights into how FtsN triggers constriction during *Escherichia coli* cell division. *Mol. Microbiol.* **95**: 903-909.

788 Willemse, J., Borst, J.W., de Waal, E., Bisseling, T., and van Wezel, G.P. (2011) Positive
789 control of cell division: FtsZ is recruited by SsgB during sporulation of *Streptomyces*.
790 *Genes Dev.* **25**: 89-99.

791 Xiao, J., and Goley, E.D. (2016) Redefining the roles of the FtsZ-ring in bacterial
792 cytokinesis. *Curr. Opin. Microbiol.* **34**: 90-96.

793 Yang, X., Lyu, Z., Miguel, A., McQuillen, R., Huang, K.C., and Xiao, J. (2017) GTPase
794 activity-coupled treadmilling of the bacterial tubulin FtsZ organizes septal cell wall
795 synthesis. *Science* **355**: 744-747.

796 Zhang, L., Willemse, J., Claessen, D., and van Wezel, G.P. (2016) SepG coordinates
797 sporulation-specific cell division and nucleoid organization in *Streptomyces coelicolor*.
798 *Open Biol* **6**: 150164.

799

800

Tables

Table 1. Phenotypes of *S. venezuelae ftsZ* mutants

Strain	*ftsZ* genotype	Colony size[‡]	Pigment[§]	Sporulation septation[¶]
ATCC 10712	*ftsZ*$^{+}$	++	+++	Regular spores
DU500	*ΔftsZ*	++	+	No spores; long non-septated hyphae
LUV044	*ΔftsZ*/*ftsZ*$^{+}$	+	+	Spores form; hyphae with septation
LUV045	*ΔftsZ*/*ftsZ*(F37S)[†]	+	+	Spores form; hyphae with septation
LUV046	*ΔftsZ*/*ftsZ*(F37R)	+(+)	+	No spores; hyphal fragments with spiral shaped septation
LUV047	*ΔftsZ*/*ftsZ*(V35A)	+	+	Spores form; hyphae with septation
LUV048	*ΔftsZ*/*ftsZ*(V35D)	+(+)	+	Spores form; hyphae with septation
LUV049	*ΔftsZ*/*ftsZ*(E36A)	(+)[#]	(+)[#]	Very poor growth; no spore formation; long hyphal fragments
LUV050	*ΔftsZ*/*ftsZ*(F37I)	++	+	No spores; hyphal fragments with spiral shaped septation
LUV051	*ΔftsZ*/*ftsZ*(GVE34-36AAA)	(+)[#]	(+)[#]	Very poor growth; no spore formation; long hyphal fragments

[†]Nucleotide changes: F37S, 110T>C; F37R, 109-110TT>CG; V35A, 104T>C; V35D, 104T>A; E36A, 107A>C; F37I, 109T>A, GVE34-36AAA, 101G>C, 104T>C, 107A>C. Nucleotide positions are numbered with respect to the first nucleotide of the start codon of *ftsZ*.

[‡]Colony size was compared with the wild type parental strain ATCC 10712 (*ftsZ*$^{+}$). ++, colony size similar to wild type. +, colonies smaller than wild type.

[§]Degree of greyish green spore pigmentation compared to wild type +++

¶Sporulation septation was estimated from phase contrast microscopic images of impression prints from aerial mycelium of developing colonies.

#Exconjugants obtained and could be cultivated on MS agar plates, but did not grow on MYM agar.

Figure legends

Figure 1. Colony phenotype of the *S. coelicolor ftsZ28* mutant. Colony appearance after 5 days of growth on MS agar. A strain with a previously described *ftsZ* allele (*ftsZ26*(Spo)) that affects production of the spore pigment is included as comparison. The *S. coelicolor* strains are: strain J2417 (*ΔftsZ* $attB_{\phi C31}$::pKF32[$ftsZ^+$]); strain O26 (*ΔftsZ* $attB_{\phi C31}$::pO26[*ftsZ26*(Spo)]; wild type parent strain M145 ($ftsZ^+$); and strain K263 (*ΔftsZ* $attB_{\phi C31}$::pKF320[*ftsZ28*]).

Figure 2. Sporulation defect in aerial hyphae of *S. coelicolor ftsZ28* mutant. Typical examples of spore chains of strain J2417 (*ΔftsZ* $attB_{\phi C31}$::pKF32[$ftsZ^+$]) (A, C, E) or aerial hyphal fragments of strain K263 (*ΔftsZ* $attB_{\phi C31}$::pKF320[*ftsZ28*] (B, D, F) from the surface of colonies after 5 days of growth on MS agar. Phase contrast micrographs (A, B), scanning electron micrographs (C, D) and transmission electron micrographs of sectioned samples (E, F). Scale bars, 2 μm.

Figure 3. Ribbon cartoon of the homology model of *S. coelicolor* FtsZ showing the location of the F37I mutation studied in this work. (A) The C-terminal activation domain and the central helix (H7) are shown in blue, the N-terminal GTPase domain, and the bound GDP are in green and orange, respectively. The phenylalanine residue affected by the mutation described in this study is indicated as spheres in grey. The homology model is based on the crystal structure of *Mycobacterium tuberculosis* FtsZ (PDB entry 1RQ7). **(B)** A detailed view of the region around helix H1 and strand S2. The F37 residue is surrounded by amino acids with hydrophobic side chains, indicated with lines. The carbon, oxygen and nitrogen atoms of the displayed amino acid side chains are depicted in green, red and blue respectively. **(C)** A sequence alignment of amino acid sequences ranging from strand S1 to helix H2, from *M. tuberculosis*, *S. coelicolor*, *E. coli* and *B. subtilis*. The secondary structure of this region is depicted above the alignment. The position of the mutations that cause twisted septa in *S. coelicolor*, *E. coli* and *B. subtilis* are indicated with boxes. All three mutations are located in strand S2 or in the loop connecting strand S2 and helix H1. As is shown below the alignment, this region is well conserved between all four bacteria. The consensus symbols below the alignment are: (*), positions which have a single, fully

conserved residue and (:), strongly conserved residues with similar properties. The sequence of *M. tuberculosis,* on which structure the homology model of *S. coelicolor* FtsZ is based, is included here as a reference. *S. venezuelae* and *S. coelicolor* FtsZ have identical sequence the displayed region.

Figure 4. **Sporulation defect in aerial hyphae of *S. venezuelae ftsZ* mutant.** Typical examples of spore chains of wild-type parent strain (*ftsZ*$^+$) **(A, E),** or aerial hyphal fragments of strain LUV050 (*ΔftsZ attB*$_{\phi BT1}$::pKF534[*ftsZ*(F37I)]) **(B, F),** strain LUV056 (*ftsZ(F37I)*) (**C, G**), or strain LUV046 (*ΔftsZ attB*$_{\phi BT1}$::pKF530[*ftsZ*(F37R)]) **(D, H)** from the surface of colonies after 5 days of growth on MYM agar. Phase contrast micrographs **(A, B, C, D),** scale bars, 5 μm, and scanning electron micrographs **(E, F, G, H)**, scale bars, 2 μm.

Figure 5. Effect of F37 mutation on Z-ring assembly in sporogenic hypha of *S. venezuelae*. (A) Cultures were grown in liquid MYM at 30ºC. Representative micrographs of sporulating hyphae visualizing FtsZ ladders in the strain LUV052 (*ftsZ*$^+$ *attB*$_{\phi BT1}$::pKF543[*ftsZ-ypet*]), and strain LUV057 (*ftsZ*(F37I) *attB*$_{\phi BT1}$::pKF544[*ftsZ*(F37I)-*ypet*]). **(B)** Montage of representative time series showing FtsZ dynamics during spore formation. Strains were grown in CellASIC ONIX microfluidic system (Merck). Fluorescence images (left) of FtsZ or FtsZ(F37I)-YPet were obtained from time-lapse microscopy and corresponding phase-contrast images are also shown (right). Top panel shows montage from strain LUV052 and bottom panel shows strain LUV057. For preparation of time montage, hyphae were straightened using ImageJ and time intervals between each image was kept at 20 min. Additionally, 0 min is set to the time when the chosen hyphae for analysis undergoes arrest of tip extension before sporulation septation commences. Scale bars, 2 μm.

Figure 6. Biochemical analyses of *S. venezuelae* FtsZ(F37I) and FtsZ(F37R). Representative results of GTPase assays **(A)** and right-angle light scattering assays of polymer formation **(B)** of the F37 mutant proteins compared to wild-type FtsZ protein. GTPase assays were performed in 3 independent experiments (n = 3) with each in duplicate and the error bars show standard deviation. Experiments were conducted at 3.5 μM FtsZ and 50 μM GTP in MMK buffer pH 6.5 at 30°C. GTPase activity was measured as release of P_i using a Malachite green assay. Light scattering intensity values are shown with arbitrary units (au).

Figure 7. Transmission electron micrographs of negatively stained *S. venezuelae* FtsZ polymers at different pH. Protein and GTP concentrations in the reactions were 3.5 μM and 500 μM, respectively. Wild-type FtsZ forms predominantly long single-stranded fibers while the F37 mutant proteins formed a mixture of polymers of short and moderate length. Scale bars, 50 nm.

Figure 8. Determination of *S. venezuelae* FtsZ critical concentration. The rate of GTP hydrolysis from GTPase assay was calculated using slopes of phosphate accumulation curves and plotted against various FtsZ concentrations. Critical concentration of the wild-type and mutant proteins is determined by extrapolating the linear regression line backwards to where it meets x-axis. The assays were performed in 2 independent experiments (n = 2). Triangles show data from wild-type FtsZ and bullets denote the F37I mutant. Open and closed symbols are used to represent data points from two independent experiments. Experiments were conducted at 30°C in HMK buffer (pH 7.7) with 500 μM GTP.

Supporting information

Additional supporting information can be found in the online version of this article at the publisher's web-site.

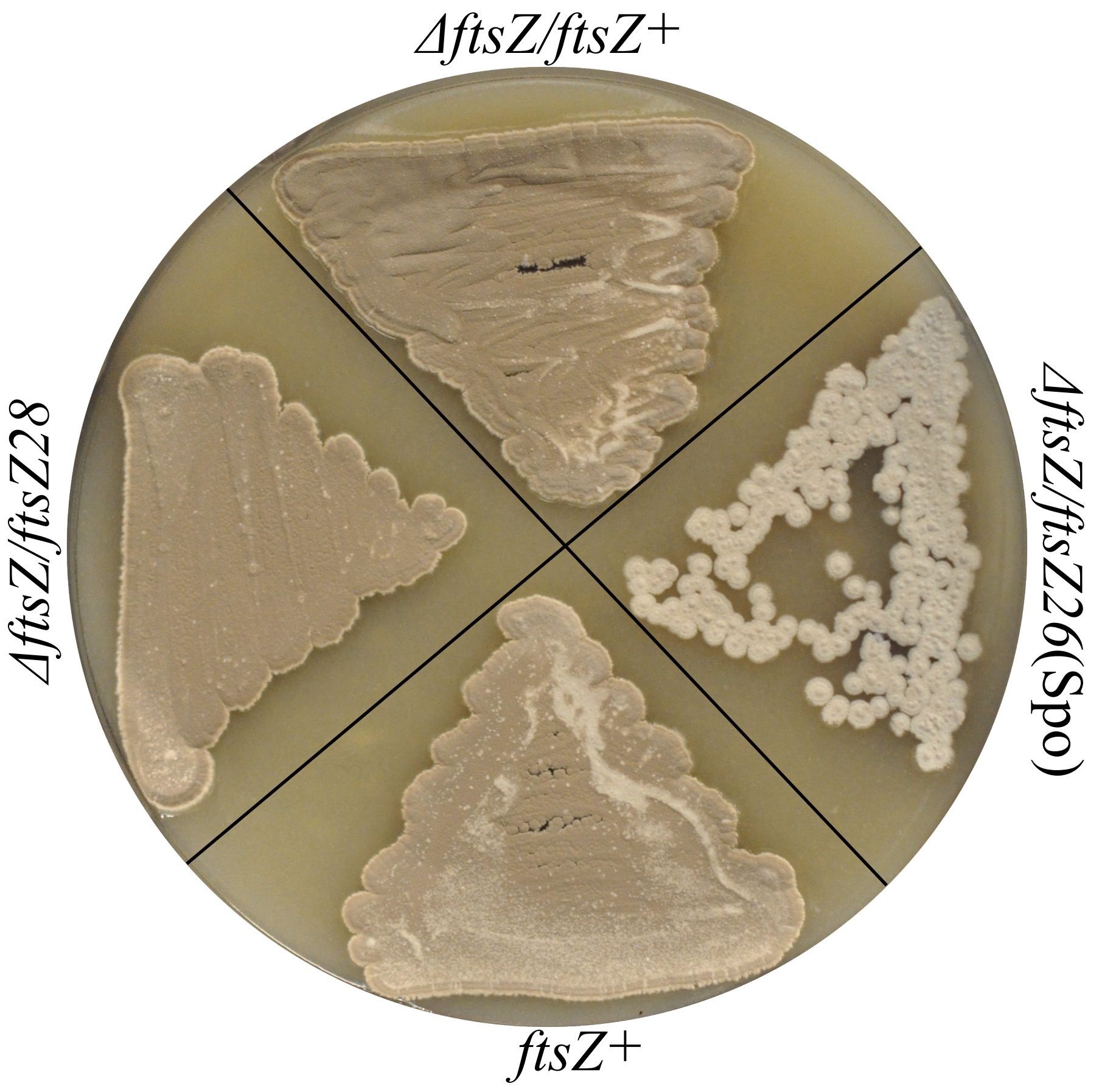
ΔftsZ/ftsZ+
ΔftsZ/ftsZ28
ΔftsZ/ftsZ26(Spo)
ftsZ+

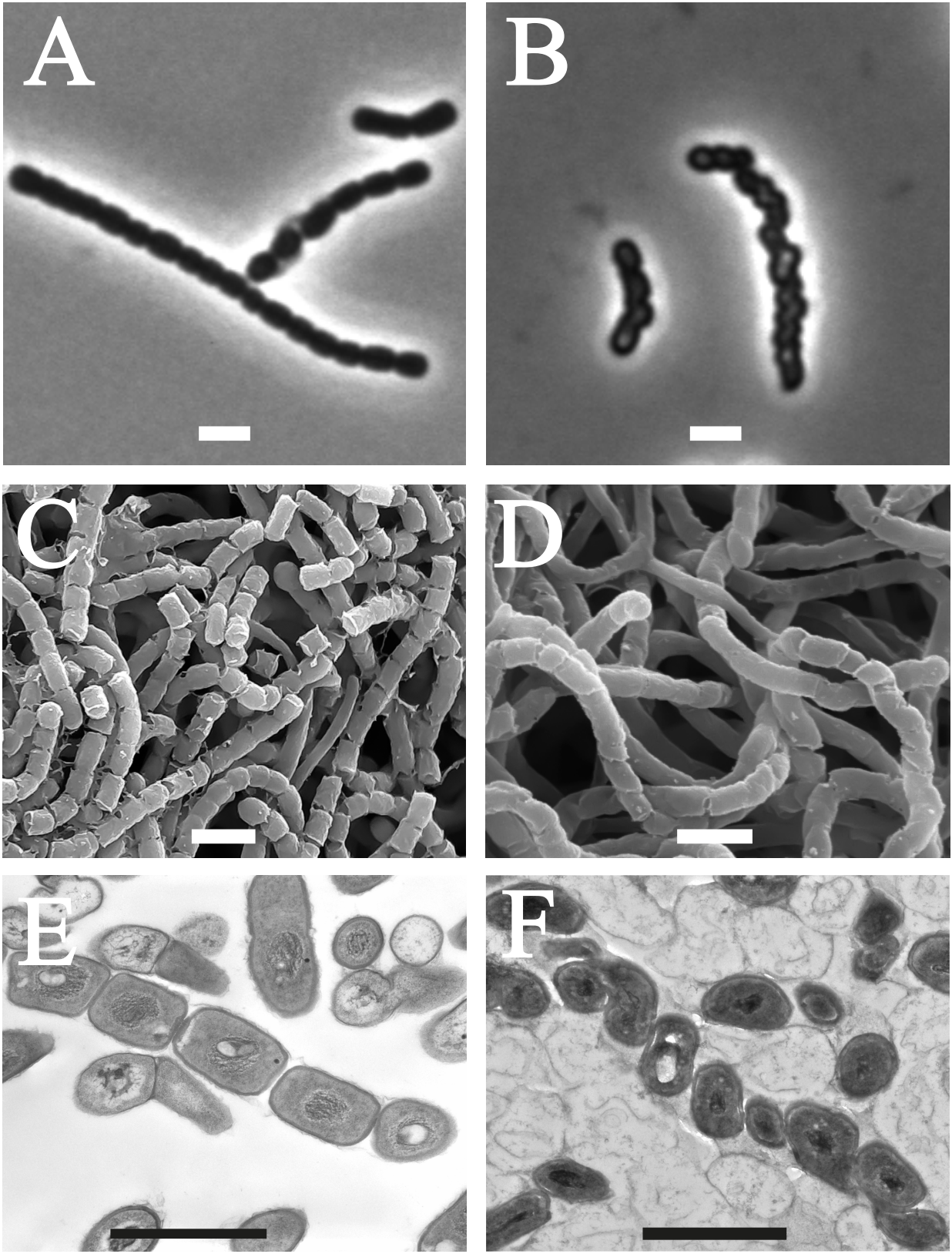
A
B
C
D
E
F

A

B

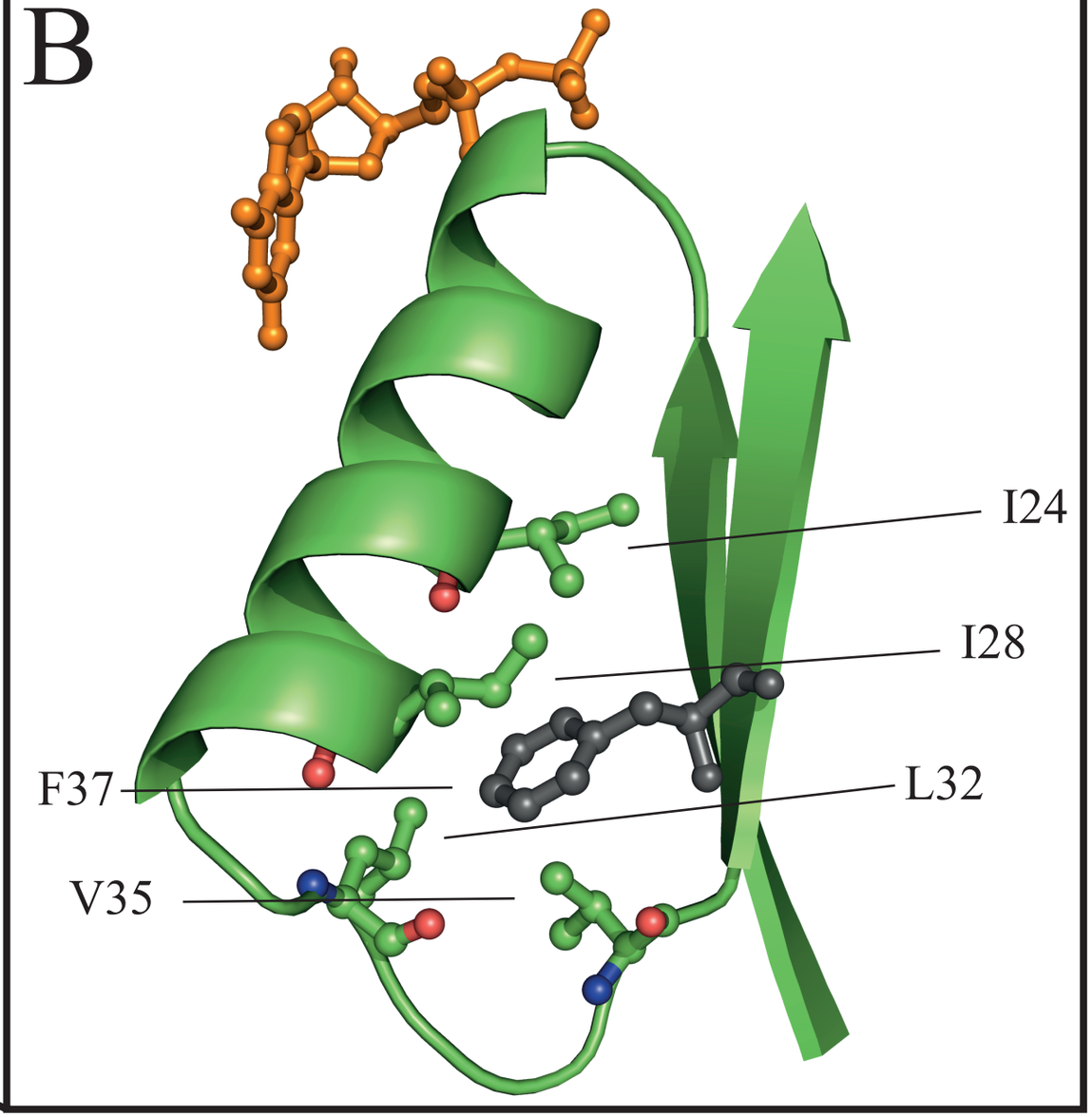

C


```
Mtb FtsZ    8  LAVIKVVGIGGGGVNAVNRMIEQGLKGVEFIAINTDAQAL  47
Sco FtsZ    8  LAVIKVIGVGGGGVNAINRMIEVGLKGVEFIAINTDAQAL  47
Eco FtsZ   10  DAVIKVIGVGGGGGNAVEHMVRERIEGVEFFAVNTDAQAL  49
Bsu FtsZ   11  LASIKVIGVGGGGNNAVNRMIENEVQGVEYIAVNTDAQAL  50
               *  ***:*:**** **:::*:.  ::***::*:*******
```

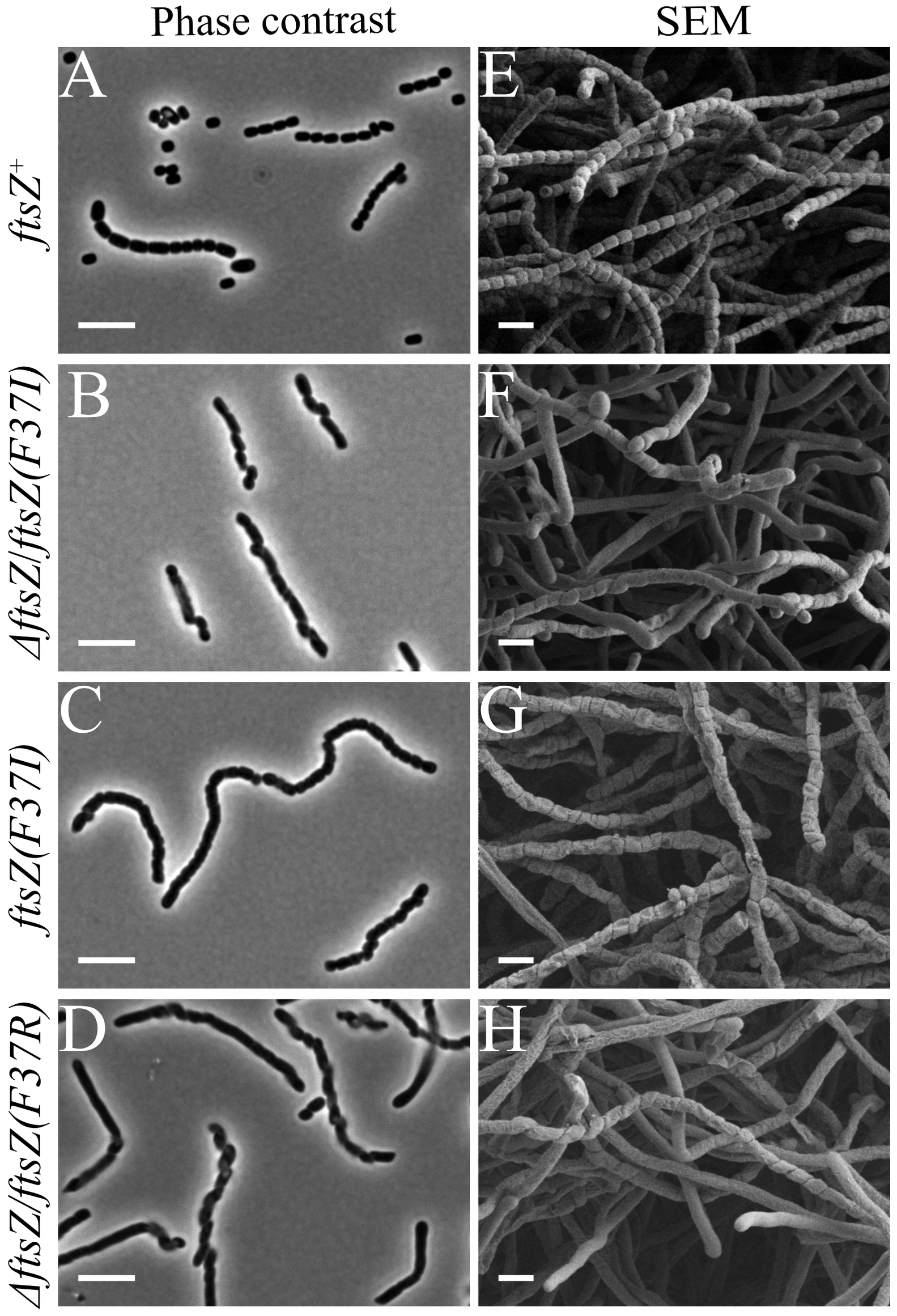
Phase contrast
SEM
A
E
ftsZ+
B
F
ΔftsZ/ftsZ(F37I)
C
G
ftsZ(F37I)
D
H
ΔftsZ/ftsZ(F37R)

A

Phase contrast

FtsZ-YPet

Merge

ftsZ^{+}*/ftsZ-ypet*

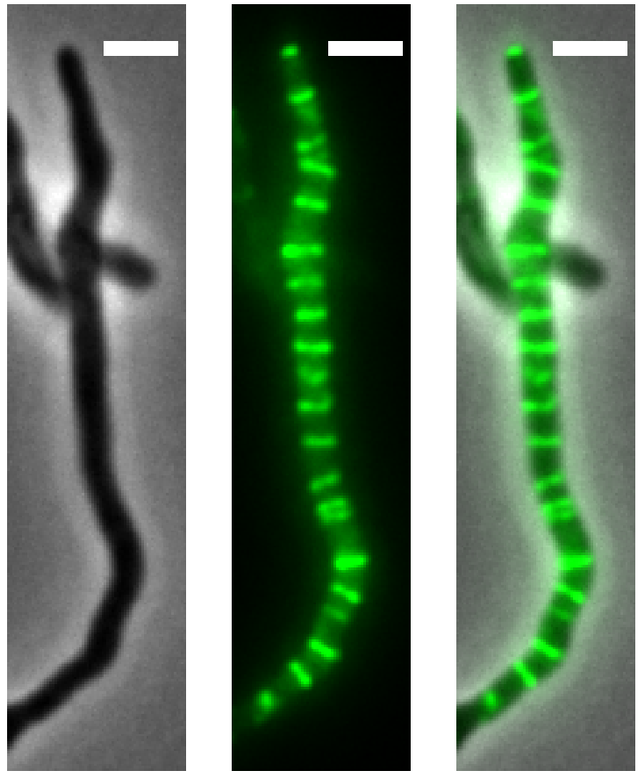

ftsZ(F37I)*/ftsZ*(F37I)*-ypet*

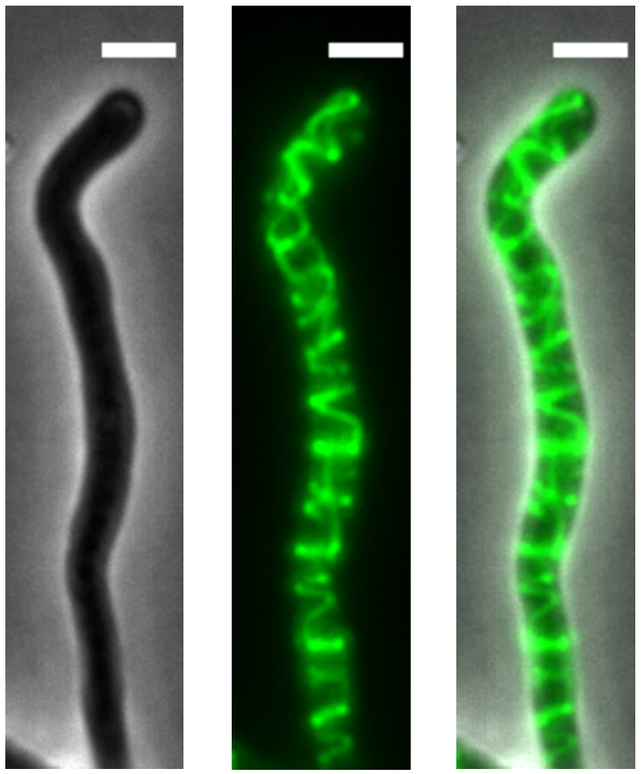

B

[min]

FtsZ-YPet

Phase contrast

ftsZ^{+}*/ftsZ-ypet*

-20
0
40
80
120
160

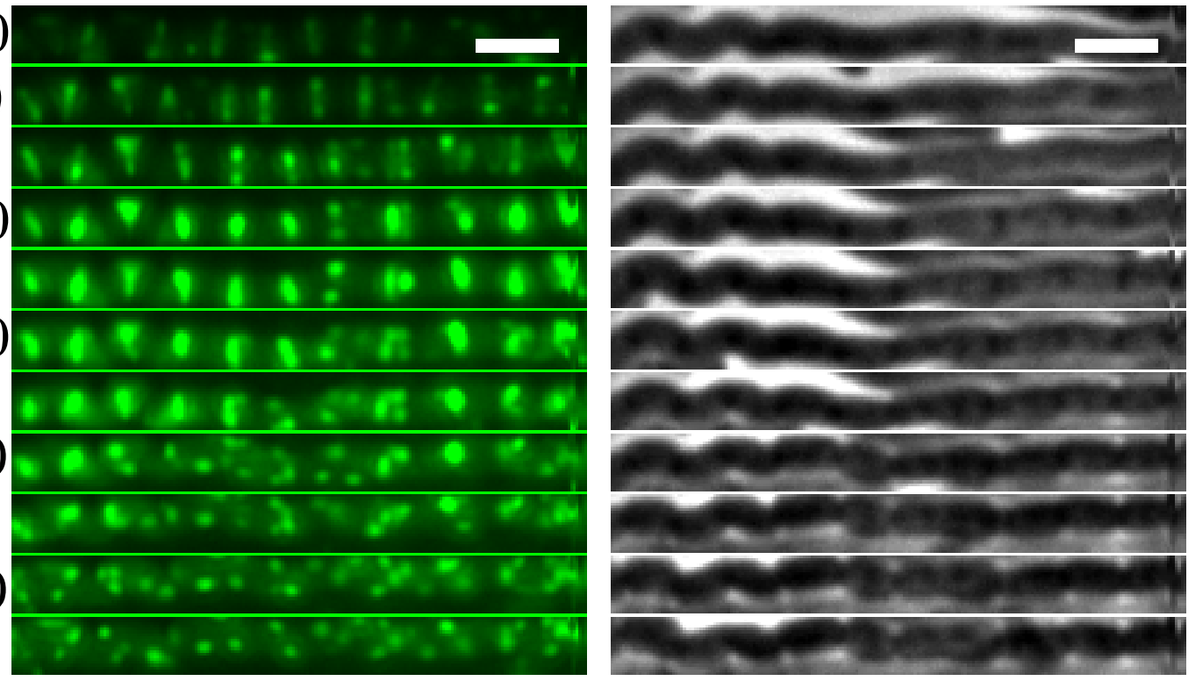

[min]

ftsZ(F37I)*/ftsZ*(F37I)*-ypet*

-20
0
40
80
120
160
200
240

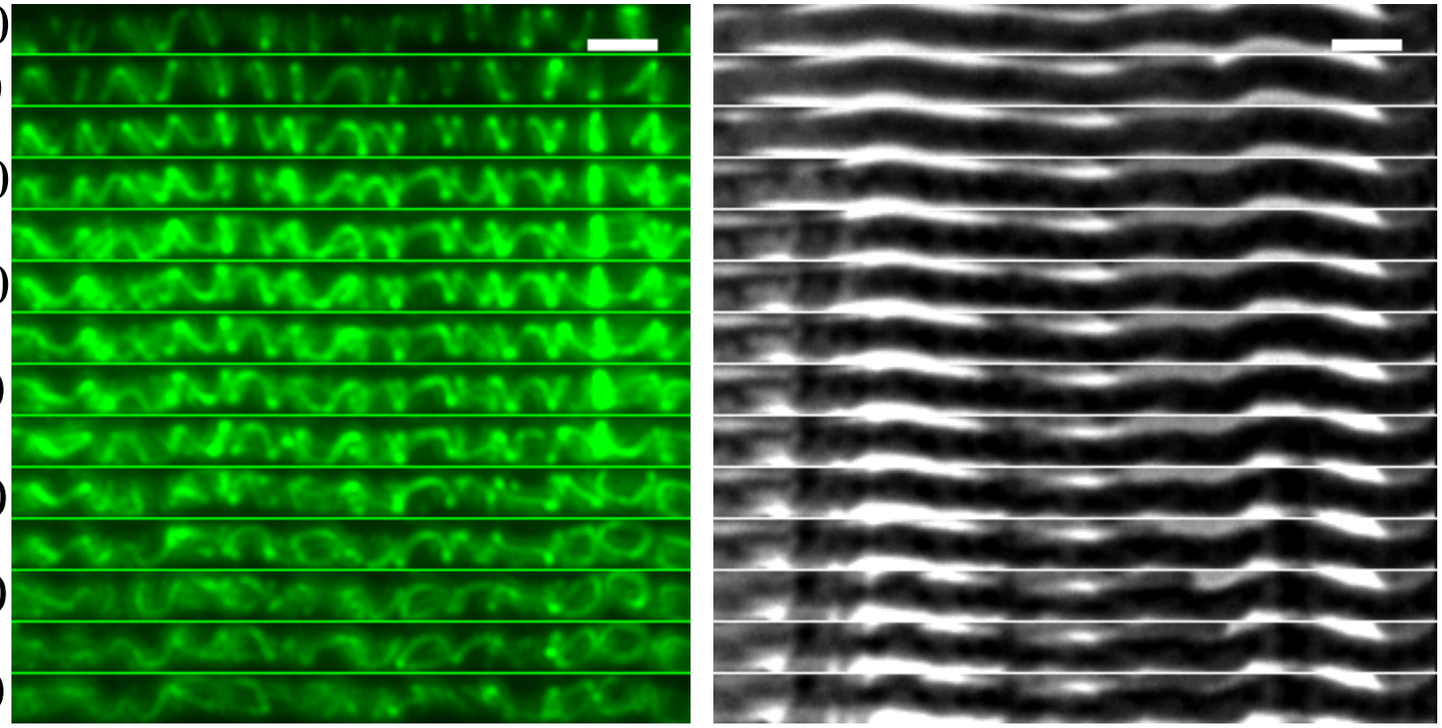

A

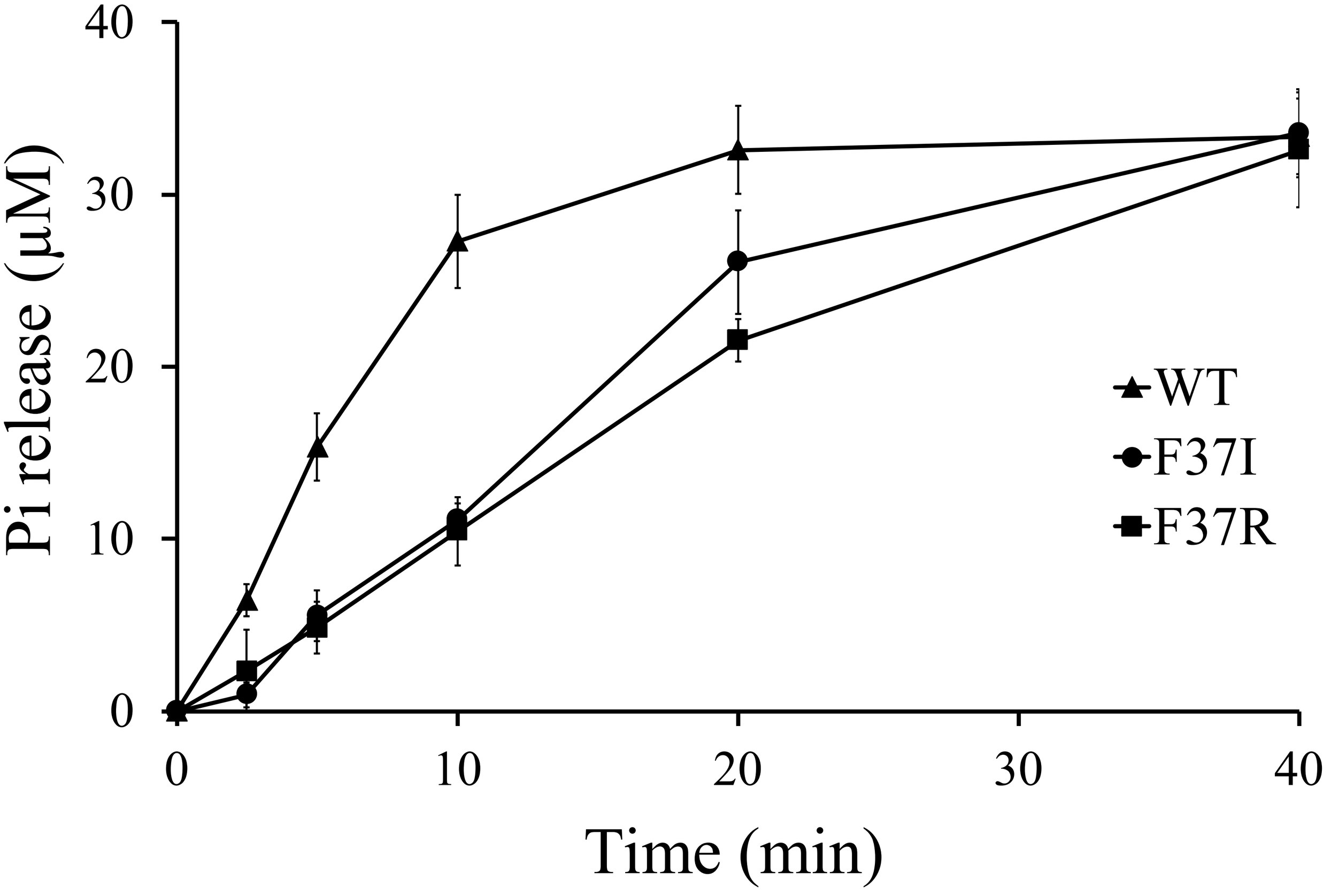
Pi release (μM)
40
30
20
10
0
0
10
20
30
40
Time (min)
WT
F37I
F37R

B

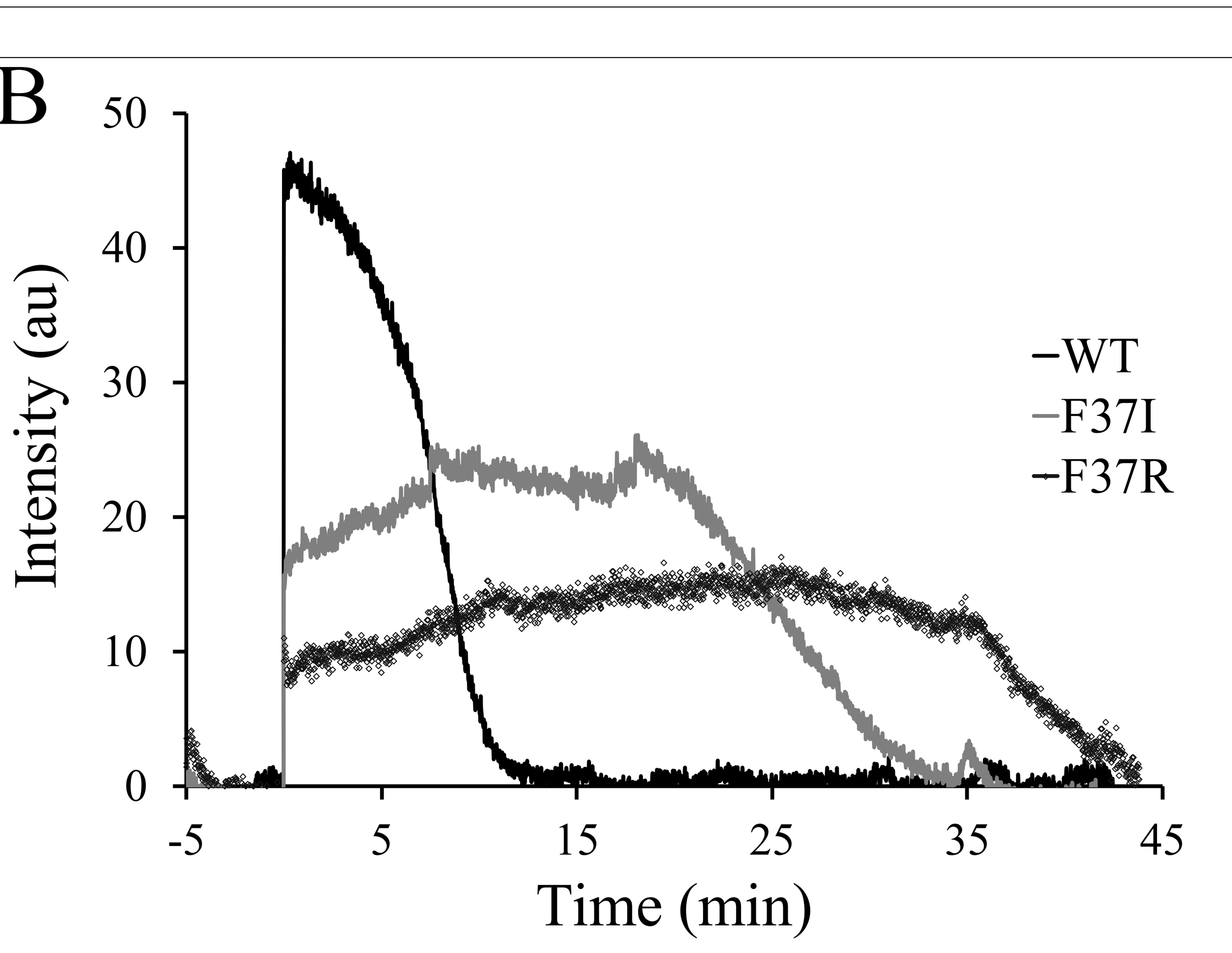
Intensity (au)
50
40
30
20
10
0
-5
5
15
25
35
45
Time (min)
WT
F37I
F37R

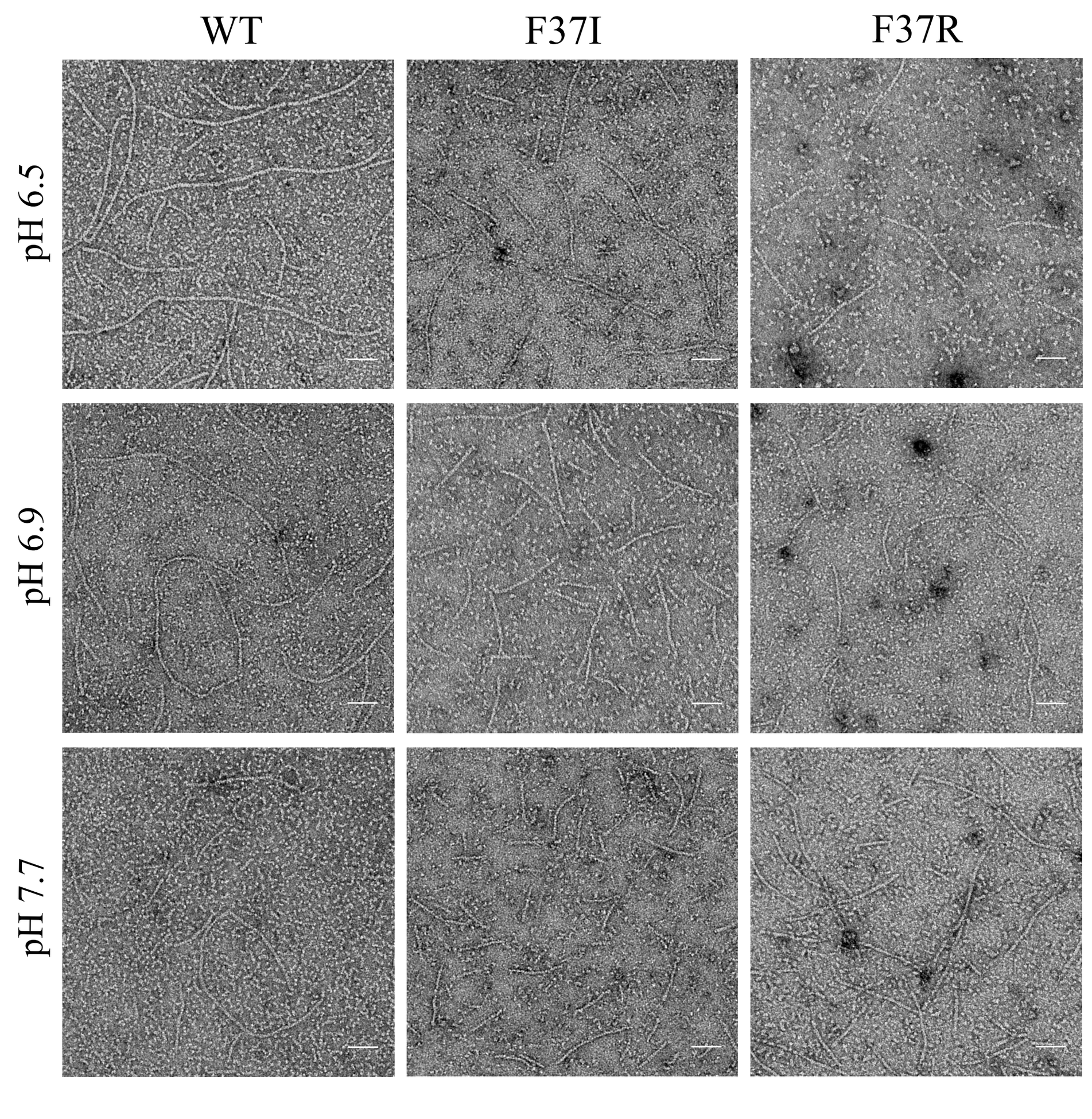
WT
F37I
F37R
pH 6.5
pH 6.9
pH 7.7

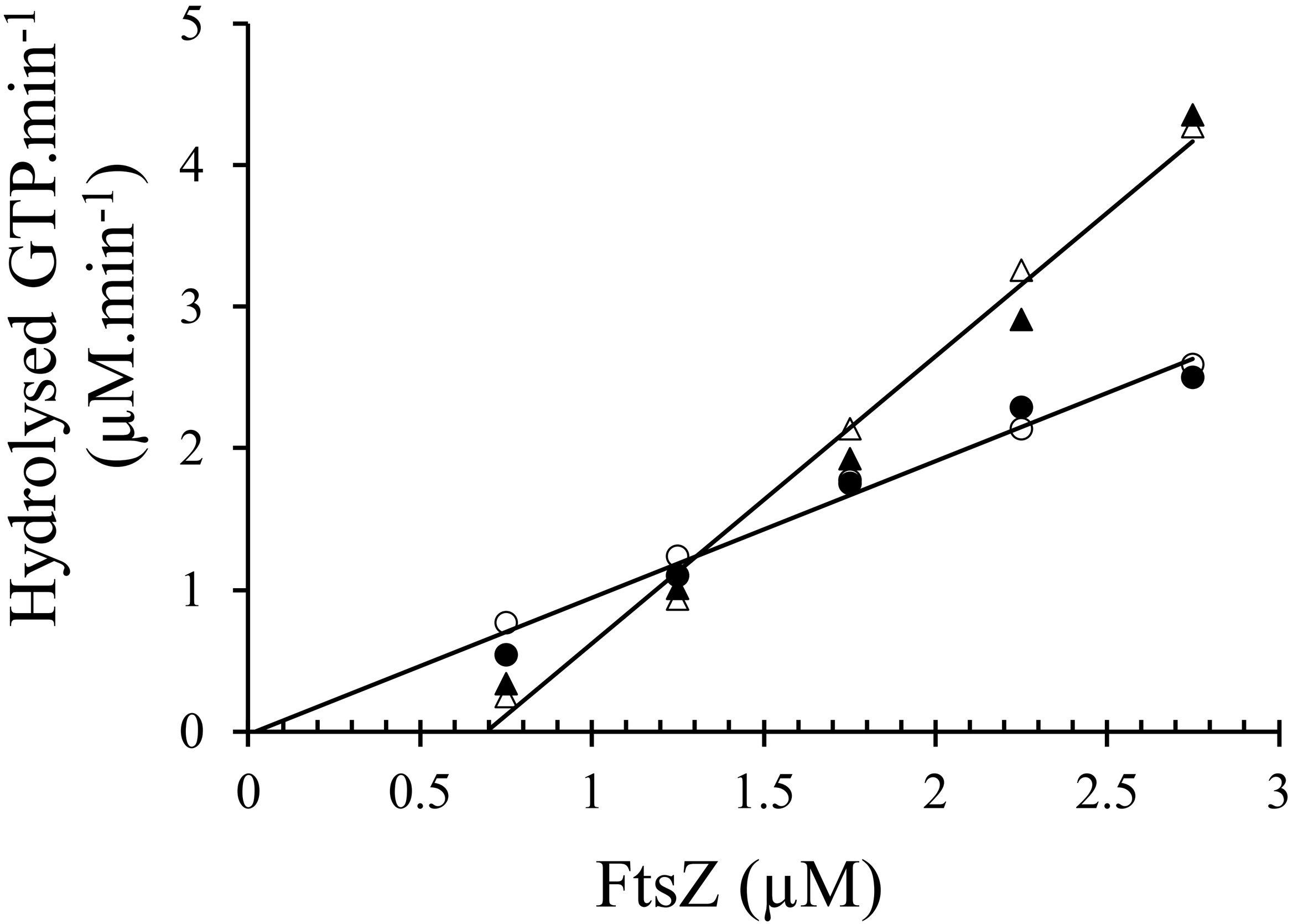
Hydrolysed GTP.min-1
(µM.min-1)
5
4
3
2
1
0
0
0.5
1
1.5
2
2.5
3
FtsZ (µM)

Supporting information

Specific amino acid substitutions in sheet S2 of FtsZ cause spiraling septation and impair assembly cooperativity in *Streptomyces* spp.

Beer Chakra Sen, Sebastian Wasserstrom, Kim Findlay, Niklas Söderholm, Linda Sandblad, Claes von Wachenfeldt, and Klas Flärdh

Table S1: Bacterial strains used in this study

Strains	Genotype or Relevant characteristics	Reference or source
Escherichia coli		
DH5α	*sup*E44 Δ*lac*U169 (*Φ80 lac*ZΔM15) *hsd*R17 *rec*A1 *end*A1 *gyr*A96 *thi*-1 *rel*A1	(Hanahan, 1983)
ER2566	Expression strain with a chromosomal copy of the T7 RNA polymerase gene	New England Biolabs
ET12567/pUZ8002	*dam*-13::Tn*9 dcm*-6 *hsd*M, carrying helper plasmid pUZ8002	(Kieser *et al.*, 2000)
***Streptomyces coelicolor* A3(2)**		
M145	Prototrophic, $SCP1^-$ $SCP2^-$ Pgl^+	(Kieser *et al.*, 2000)
HU133	*ΔftsZ::aphI*	(McCormick *et al.*, 1994)
J2417	*ΔftsZ::aphI* $attB_{\phi C31}$::pKF32[$ftsZ^+$]	(Flärdh *et al.*, 2000)
O26	*ΔftsZ::aphI* $attB_{\phi C31}$::pO26[*ftsZ26*(Spo)]	(Wasserstrom *et al.*, 2013)
K263	*ΔftsZ::aphI* $attB_{\phi C31}$::pKF320[*ftsZ28*]	This work
Streptomyces venezuelae		
NRRL B-65442	wild-type *S. venezuelae* strain	(Bush *et al.*, 2019)
DU500	*ΔftsZ*::*apr*[1]	J.R. McCormick, Duquesne University, USA
LUV044	*ΔftsZ*:: *apr* $attB_{\phi BT1}$::pSS193[$ftsZ^+$]	This work
LUV045	*ΔftsZ*:: *apr* $attB_{\phi BT1}$::pSS529[*ftsZ*(F37S)]	This work
LUV046	*ΔftsZ*::*apr* $attB_{\phi BT1}$::pKF530[*ftsZ*(F37R)]	This work
LUV047	*ΔftsZ*::*apr* $attB_{\phi BT1}$::pSS531[*ftsZ*(V35A)]	This work
LUV048	*ΔftsZ*::*apr* $attB_{\phi BT1}$::pSS532[*ftsZ*(V35D)]	This work
LUV049	*ΔftsZ*::*apr* $attB_{\phi BT1}$::pSS533[*ftsZ*(E36A)]	This work
LUV050	*ΔftsZ*::*apr* $attB_{\phi BT1}$::pKF534[*ftsZ*(F37I)]	This work
LUV051	*ΔftsZ*::*apr* $attB_{\phi BT1}$::pKF535[*ftsZ*(GVE34-36AAA)]	This work
LUV052	$attB_{\phi BT1}$::pKF543[*ftsZ-ypet*]	This work
LUV056	*ftsZ*(F37I)	This work
LUV057	*ftsZ*(F37I) $attB_{\phi BT1}$::pKF544[*ftsZ*(F37I)-*ypet*]	This work

[1]*apr* here denotes a cassette containing both the apramycin resistance gene *aac(3)IV* and an *oriT*

Table S2: Plasmids used in this study

Vector/ construct	Description[1]	Reference or source
pGus21	Cloning vector, *gusA*, Apra^r	G. Muth, Universität Tübingen, Germany
pIJ10770	Derivative of pMS82, Hyg^r	(Schlimpert *et al.*, 2017)
pKF32	Integrating vector (ΦC31 *attB*) carrying *S. coelicolor ftsZ* and its native promoter region, Apra^r	(Flärdh *et al.*, 2000)
pKF176	Expression plasmid for *S. coelicolor* FtsZ fused to intein and a chitin-binding domain.	(Wasserstrom *et al.*, 2013)
pKF320	Plasmid carrying S. *coelicolor ftsZ*(F37I) allele, isolated from *ftsZ* mutants defective in sporulation.	This paper
pKF328	Expression plasmid for *S. coelicolor* FtsZ(F37I) constructed by site-directed mutagenesis of pKF176	This paper
pKF351	Mobilisable plasmid integrating as a single copy at the ΦC31 *attB* attachment site, and carrying an *ftsZ-ypet* fusion under the control of native *ftsZ* promoters, Apra^r	(Donczew *et al.*, 2016)
pKF529	Derivative of pSS193 with *S. venezuelae ftsZ*(F37S) allele, generated by site-directed mutagenesis, Hyg^r	This work
pKF530	Derivative of pSS193 with *S. venezuelae ftsZ*(F37R) allele, generated by site-directed mutagenesis, Hyg^r	This work
pKF531	Derivative of pSS193 with *S. venezuelae ftsZ*(V35A) allele, generated by site-directed mutagenesis, Hyg^r	This work
pKF532	Derivative of pSS193 with *S. venezuelae ftsZ*(V35D) allele, generated by site-directed mutagenesis, Hyg^r	This work
pKF533	Derivative of pSS193 with *S. venezuelae ftsZ*(E36A) allele, generated by site-directed mutagenesis, Hyg^r	This work
pKF534	Derivative of pSS193 with *S. venezuelae ftsZ*(F37I) allele, generated by site-directed mutagenesis, Hyg^r	This work
pKF535	Derivative of pSS193 with *S. venezuelae ftsZ*(GVE34-36AAA) allele, generated by site-directed mutagenesis, Hyg^r	This work
pKF540	Derivative of pKF351 encoding FtsZ(F37I)-Ypet fusion, Apra^r	This work
pKF541	Expression plasmid for *S. venezuelae* FtsZ in pTYB2, Amp^r	This work
pKF542	Expression plasmid for *S. venezuelae* FtsZ(F37I) in pTYB2, Amp^r	This work

pKF543	Derivative of pIJ10770 encoding *S. venezuelae* FtsZ-Ypet fusion, Hyg^r	This work
pKF544	Derivative of pIJ10770 encoding *S. venezuelae* FtsZ(F37I)-Ypet fusion, Hyg^r	This work
pKF546	Expression plasmid for *S. venezuelae* FtsZ(F37R) in pTYB2, Amp^r	This work
pKF550	pUC18 derivative containing *S. venezuelae ftsZ* allele with 1500 flanking bases upstream-downstream of codon for F37, Amp^r	This work
pKF606	Derivative of pKF550 containing *S. venezuelae ftsZ*(F37I) allele with 1500 flanking bases upstream-downstream of mutated codon, Amp^r	This work
pKF608	Derivative of pGus21 containing *S. venezuelae ftsZ*(F37I) allele with 1500 flanking bases upstream-downstream of mutated codon from pKF606, Apra^r	This work
pMS82	Vector that integrates at ΦBT1 *attB* site, Hyg^r	(Gregory *et al.*, 2003)
pSS193	Derivative of pIJ10770 containing *S. venezuelae ftsZ*, Hyg^r	Susan Schlimpert, JIC, Norwich, UK
pTYB2	Expression vector containing gene for self-cleavable intein tag and a chitin-binding domain	New England Biolabs

[1]Amp^r, ampicillin resistance; Apra^r, apramycin resistance; Hyg^r, Hygromycin resistance

Table S3: Primers used in this study

Primers	Sequence (5'→3')[1]	Comments
KF44	AGGCCTTC**C**A**T**ATGGCAGCACCGCA[2]	Cloning of *S. venezuelae ftsZ* or *ftsZ*(F37I) *or ftsZ*(F37R) into pTYB2; forward
KF879	AAGGGCGTCGAG**A**TCATCGCCATC	Site-directed mutagenesis to introduce *ftsZ*(F37I) in pKF176; forward
KF880	GAGACCGACCTCGATCATCCGGTT	Site-directed mutagenesis to introduce *ftsZ*(F37I) in pKF176; reverse
KF1242	**A**TCATCGCGATCAACACCGACGC	F37I; forward
KF1243	T**C**CATCGCGATCAACACCGACG	F37S; forward
KF1244	CTCGACGCCCTTGAGACCGA	F37I, F37S and F37R; reverse
KF1245	CGGGAGGTTCGGCGTGTTCGTTG	Sequencing *ftsZ*; forward
KF1246	CCTCTGACCCCTGACCCCGTC	Sequencing *ftsZ*; reverse 1
KF1254	**CG**CATCGCGATCAACACCGACG	F37R; forward
KF1255	**C**CGAGTTCATCGCGATCAACACCG	V35A; forward
KF1256	CGCCCTTGAGACCGACCTCG	V35A and V35D; reverse
KF1257	**A**CGAGTTCATCGCGATCAACACCG	V35D; forward
KF1258	**C**GTTCATCGCGATCAACACCGAC	E36A; forward
KF1259	CGACGCCCTTGAGACCGACC	E36A; reverse
KF1260	**C**CG**C**CG**C**GTTCATCGCGAT	GVE34-36AAA; forward
KF1261	CCTTGAGACCGACCTCGATCA	GVE34-36AAA; reverse
KF1266	GTTCGCCCCGGCCCCGAG	Sequencing *ftsZ*; reverse 2
KF1273	GGCGGCTCTAGAGGGGTCTGACGCTC AGTGGAACG[3]	Cloning *S. venezuelae ftsZ*(F37I) or *ftsZ*(F37R) into pKF351 and/or pIJ10770; forward
KF1274	GGCGGCCATATGGCCACCGCCCCCCT TCAGGAAGTCCGGGACGTCCAG	Construction of FtsZ(F37I)-Ypet in pIJ10770; reverse
KF1277	CTTCAGGAAGTCCGGGACGTCCAG	Cloning *S. venezuelae ftsZ* or *ftsZ*(F37I) into pTYB2; reverse
KF1290	GGCGGCAAGCTTCGGACCGGTTGCTC CAGGAG	Construction of FtsZ-Ypet into pIJ10770; forward
KF1291	GGCGGCCCTAGGTTACTTATAGAGCT CGTTCATGCCCTCG	Construction of FtsZ-Ypet or FtsZ(F37I)-Ypet into pIJ10770; reverse
KF1377	GGCGGCTCTAGAATGACCGTCGCCGA GCTCTC	Cloning of *ftsZ* flanking 1500 bases upstream of F37 mutation into pUC18; forward
KF1378	GGCGGCGAATTCTTCACCATCGCCCC GACC	Cloning of *ftsZ* flanking 1500 bases upstream of F37 mutation into pUC18; reverse
T7 universal	TAATACGACTCACTATAGGG	Forward sequencing primer (New England Biolabs)
Intein Reverse	ACCCATGACCTTATTACCAACCTC	Reverse sequencing primer (New England Biolabs)

[1]Bold underlined nucleotides denote exchanged base for site-directed mutagenesis
[2]The two bold underlined nucleotides were changed to introduce an NdeI site at the start codon of *ftsZ*
[3]The underlined regions denote different restriction sites.

Supplementary Figures

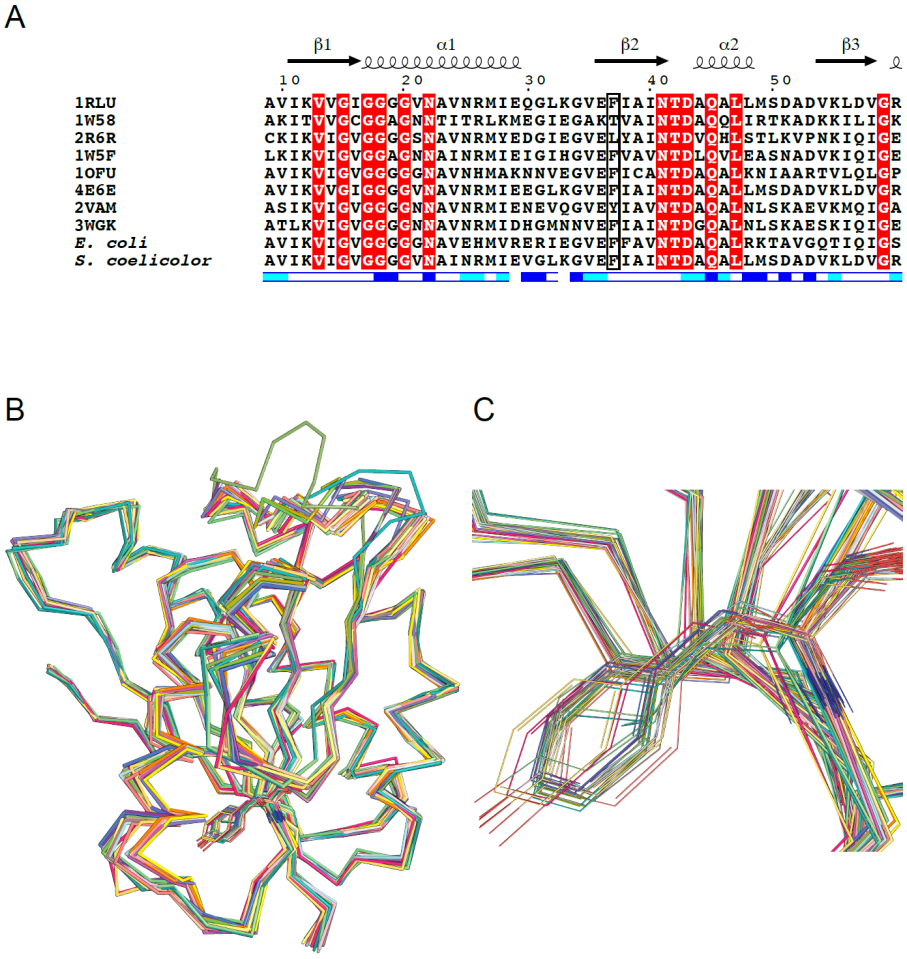

Figure S1. Sequence and structural alignment of FtsZ. (**A**) Multiple sequence alignment of the N-terminal region of FtsZ proteins with crystal structures from *Mycobacterium tuberculosis* (PDB ID 1RLU), *Methanocaldococcus jannaschii* (PDB ID 1W58), *Aquiflex aeolicus* (PDB ID 2R6R), *Thermotoga maritima* (PDB ID 1W5F), *Pseudomonas aeruginosa* (PDB ID 1OFU), *Thermobifida fusca* (PDB ID 4E6E), *Bacillus subtilis* (PDB ID 2VAM), and *Staphylococcus aureus* (PDB ID 3WGK). *E. coli* (*Escherichia coli*, UniProtKB: P0A9A6), *S. coelicolor* (*Streptomyces coelicolor,* UniProtKB*:* P45500). The secondary structure elements derived from the structure of *M. tuberculosis* (PDB ID 1RLU) are indicated above the sequence. The alignment was obtained using T-COFFE (Di Tommaso *et al.*, 2011) and annotated using ESPript (Robert & Gouet, 2014). White characters on a red background indicate strictly conserved residues. The position corresponding to F37 of *S. coelicolor* FtsZ is boxed. Accessibility of *M. tuberculosis* (PDB ID 1RLU) is shown by a bar below the sequences: blue is accessible, cyan is intermediate, white is buried. (**B**) Structural alignment of 25 FtsZ proteins. The following FtsZ structures were obtained from the Protein Data Bank: PDB IDs 1RLU, 1FSZ, 1W58, 1W59, 1W5A, 1W5B, 1W5E, 2VAP, 2R6R, 2R75, 1OFU, 2VAW, 1RQ2, 1RQ7, 2Q1X, 2Q1Y, 4KWE, 4E6E, 2VAM, 2RHH, 2RHJ, 2RHL, 2RHO, 2VXY, 4U39, 3WGK, 3WGL, 3VOA, 3VOB, 3VO8, 4DXD, 3WGM, 3WGN, 3WGJ, 5MN4, 5MN5, 5MN6, 5MN7, 5MN8, 4M8I. The N-terminal domain (corresponding to residues 9 to 163 of PDB ID 1RLU) of chain A from each structure were aligned with 1RLU using PyMOL and the command *align*. The aligned structures are shown in ribbon representations. The

Cα root mean square deviation for all structures versus PDB ID 1RLU was less than 0.7Å. (**C**) Close up of the side chain position corresponding to F37.

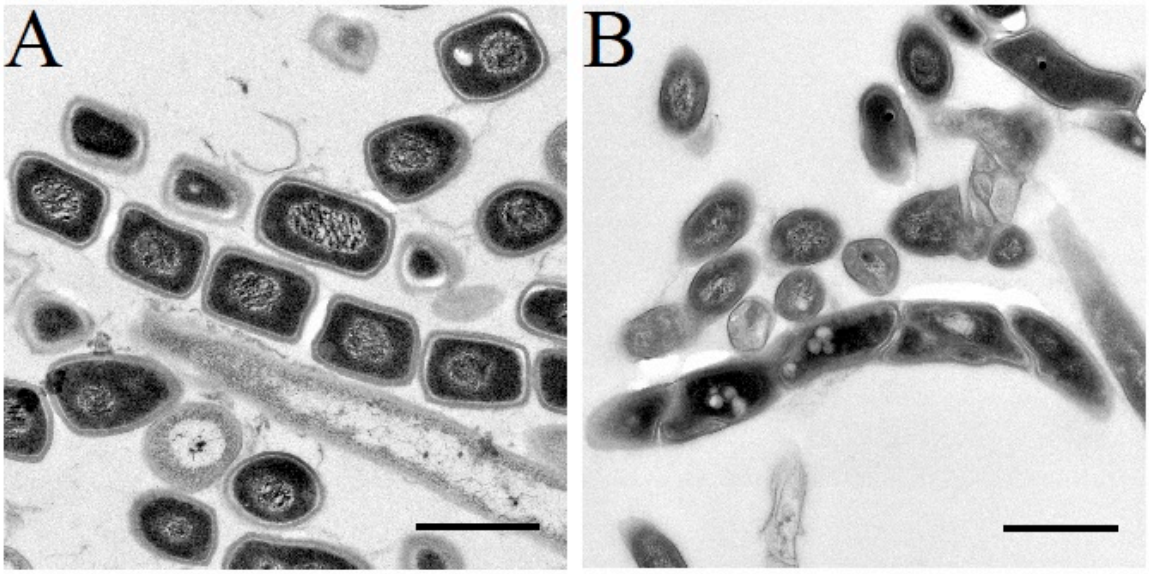

Figure S2. Sporulation defect in aerial hyphae of *S. venezuelae ftsZ*(F37I) mutant. Transmission electron micrographs of sectioned samples of **(A)** spore chains of wild type parent strain ATCC10712 (*ftsZ*$^{+}$) or **(B)** aerial hyphal fragments of strain LUV050 (*ΔftsZ attB*$_{\phi BT1}$*::*pKF534[*ftsZ*(F37I)]) from the surface of colonies after 5 days of growth on MYM agar. Scale bars, 1 μm.

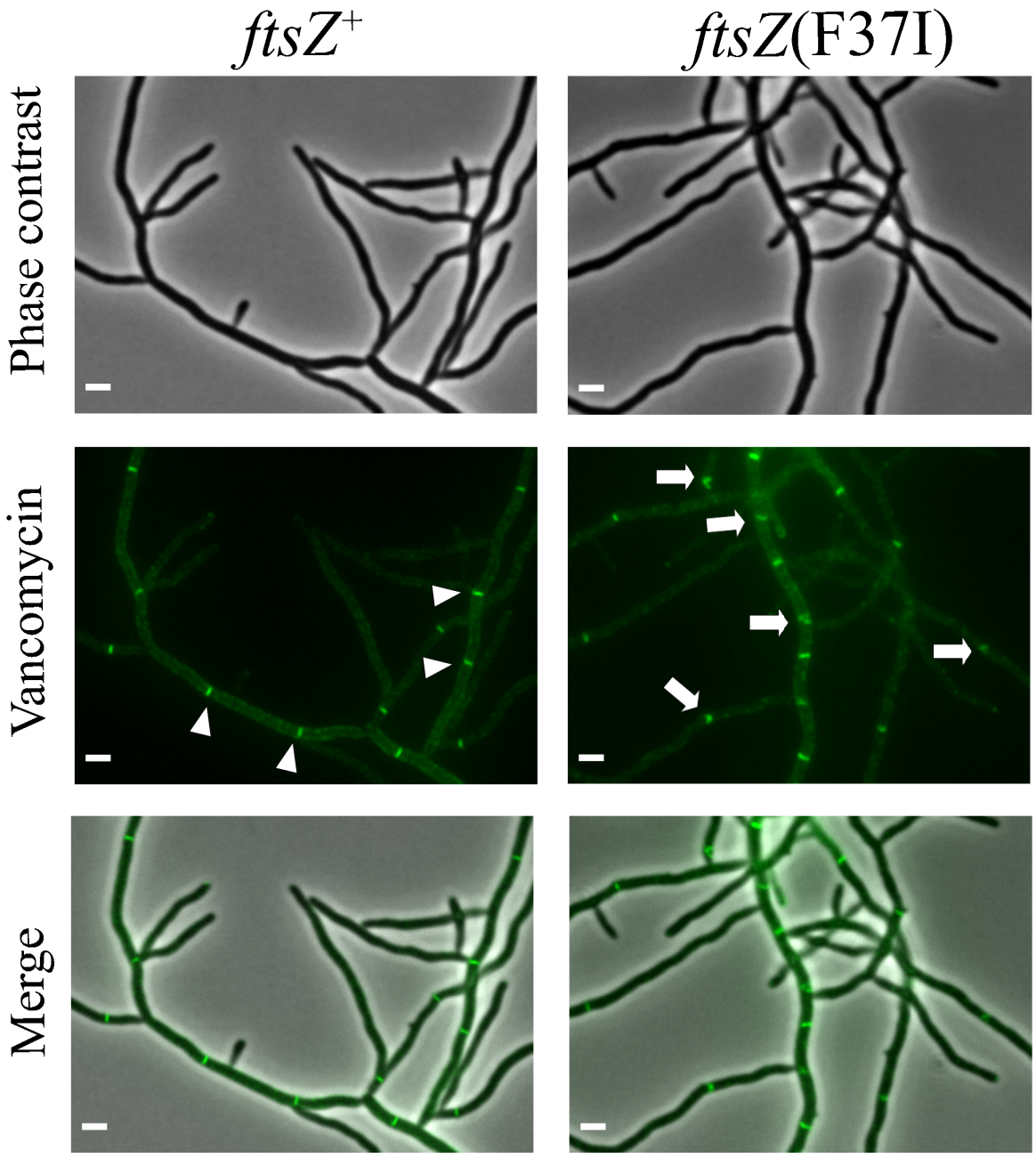

Figure S3. Formation of hyphal cross-walls in vegetatively growing hyphae of *S. venezuelae*. Cultures were grown in liquid MYM at 30ºC and stained with BODIPY FL vancomycin conjugate (in green). Representative micrographs showing some clear examples of, (left) regular hyphal cross-walls (shown with arrowheads) in wild type strain (*ftsZ*+), and (right) perturbed cross-walls (shown with arrows) in LUV056 (*ftsZ*(F37I)). Scale bars, 2 μm.

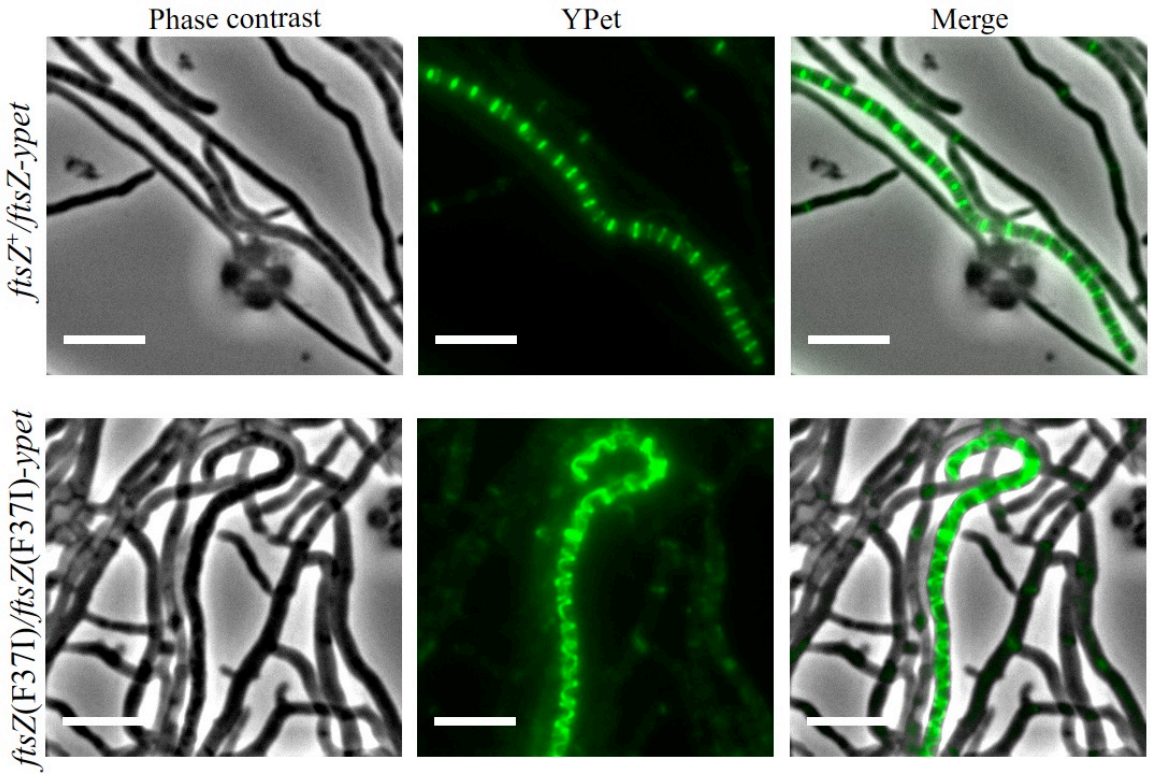

Figure S4. Representative snapshot images from time-lapse fluorescence microscopy of *S. venezuelae* showing fluorescently labeled FtsZ. Cultures were grown in microfluidics chambers in MYM at 30ºC. Images shown are selected frames (of Supplementary Movies 1 and 2) of sporulating hyphae visualizing FtsZ ladders (shown in green) in strain LUV052 (*ftsZ*$^{+}$ *attB*$_{\phi BT1}$*::*pKF543[*ftsZ-ypet*]) or YPet-tagged FtsZ(F37I) in strain LUV057 (*ftsZ*(F37I) *attB*$_{\phi BT1}$*::*pKF544[*ftsZ*(F37I)-*ypet*]). Scale bars, 5 μm.

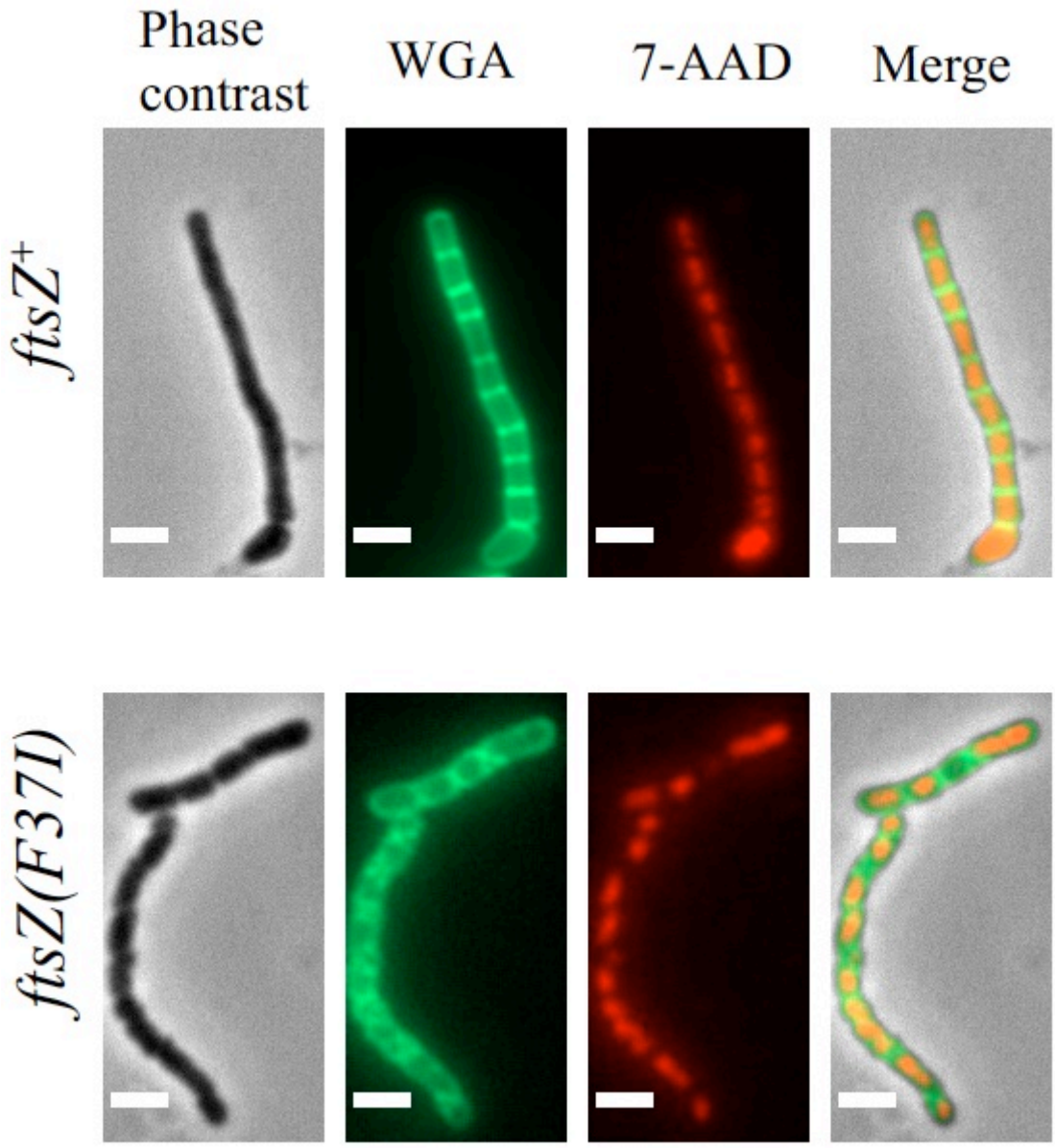

Figure S5. Effect of F37 mutation in sporulating hyphae of *S. venezuelae*. Cultures were grown in liquid MYM at 30ºC and stained with cell wall stain WGA-Oregon green (in green) and DNA stain 7-AAD (in red). Representative micrographs of sporulating aerial hyphal fragments of wild type strain (*ftsZ*+), and in LUV056 (*ftsZ*(F37I)). Scale bars, 2 μm.

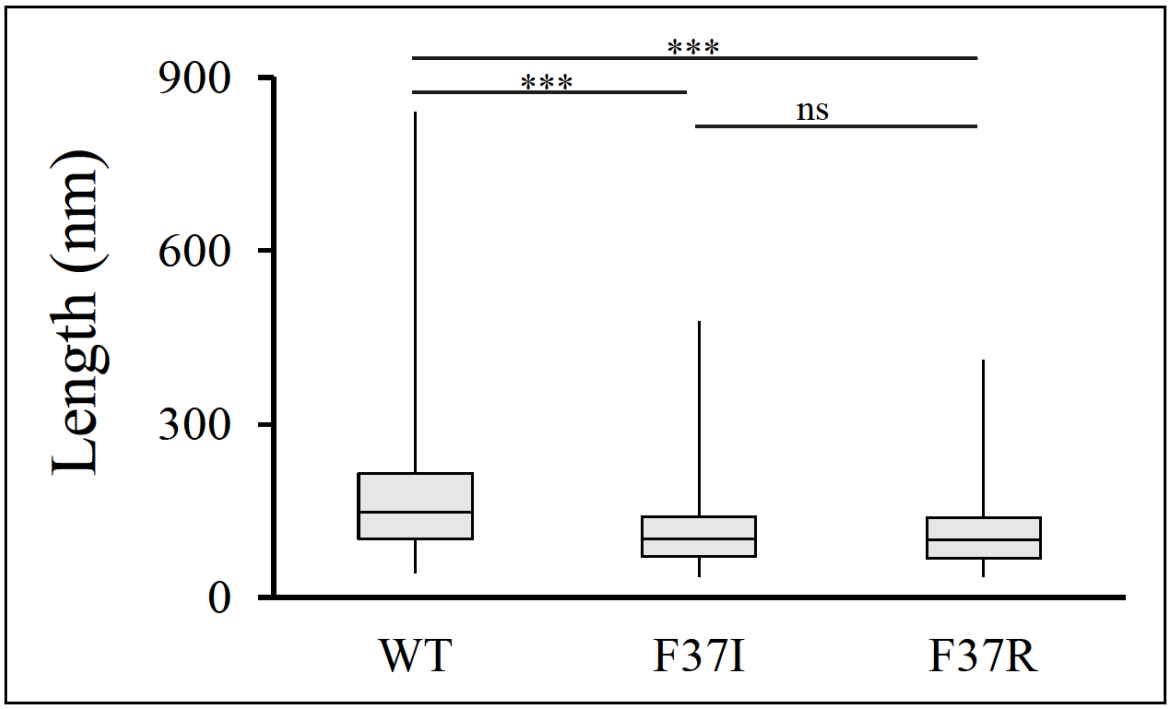

Figure S6. FtsZ protofilaments length determination. Transmission electron micrographs of negatively stained *S. venezuelae* FtsZ polymers (obtained from pH 6.5 condition, see Fig. 7) were imported to Fiji software. Using drawing tools, three hundred measurements were made from more than 7 micrographs for each of the proteins. While choosing filaments for length measurements, only those filaments which were within the imaging field were considered. Statistical significance was calculated using two-tailed unpaired *t*-test and filament length distributions was plotted. Data are mean and s.d. ***$P < 0.001$. ns denotes no significance ($P > 0.05$).

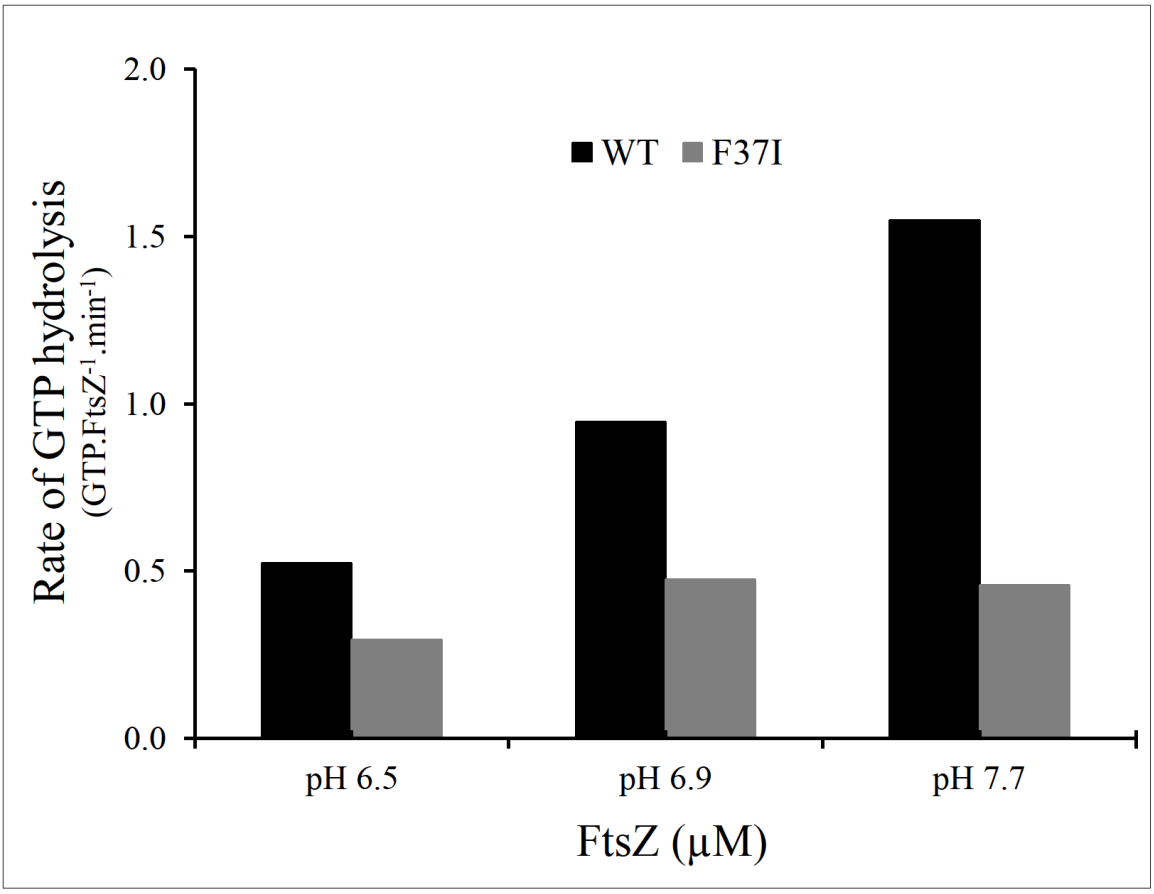

Figure S7. Effect of pH on GTPase activity of *S. coelicolor* FtsZ. Representative results from GTPase assay of *S. coelicolor* FtsZ (wild type) and FtsZ(F37I) at various pH conditions. All assays were performed at 30°C with final concentration of FtsZ at 3.5 µM and GTP at 50 µM. The different buffers were MES (pH 6.5), MOPS (pH 6.9) and HEPES (pH 7.7) with 10 mM MgAc and 200 mM KAc in all cases. A single experiment (n = 1) was performed.

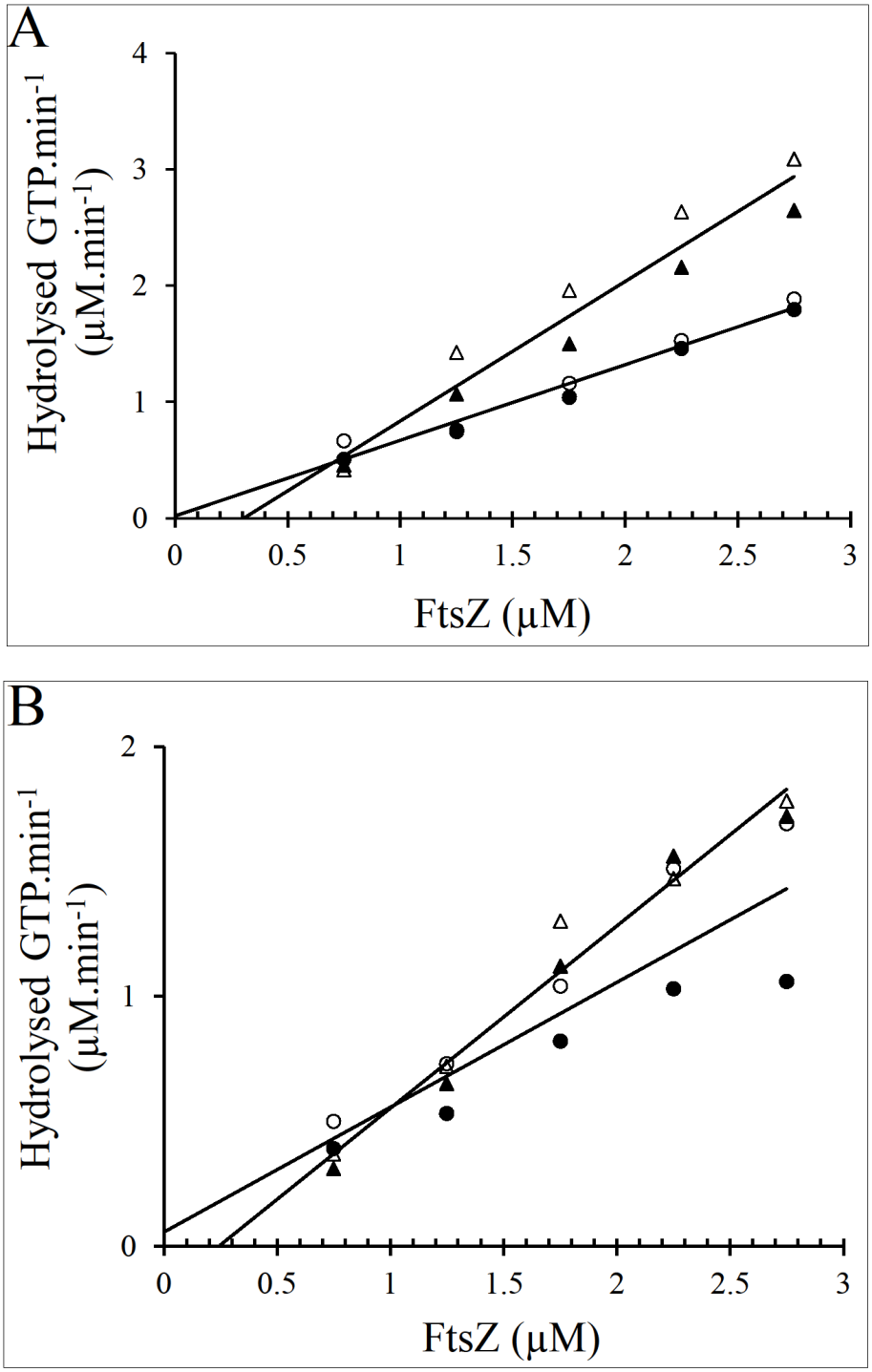

Figure S8. Determination of *S. venezuelae* and *S. coelicolor* FtsZ critical concentration. The rate of GTP hydrolysis from GTPase assay was calculated using slopes of phosphate accumulation curves and plotted against various FtsZ concentrations (as described in Experimental procedures). Critical concentration of the wild type and mutant FtsZ proteins, of *S. venezuelae* **(A)** and *S. coelicolor* **(B)** is determined by extrapolating the linear regression line backwards to where it meets x-axis. Triangles (open and close) and bullets (open and close) represent data points from two independent experiments, for wild-type protein and F37I mutant protein, respectively. All experiments were conducted, in duplicate, at 30°C in MMK buffer (pH 6.5) with 500 µM GTP.

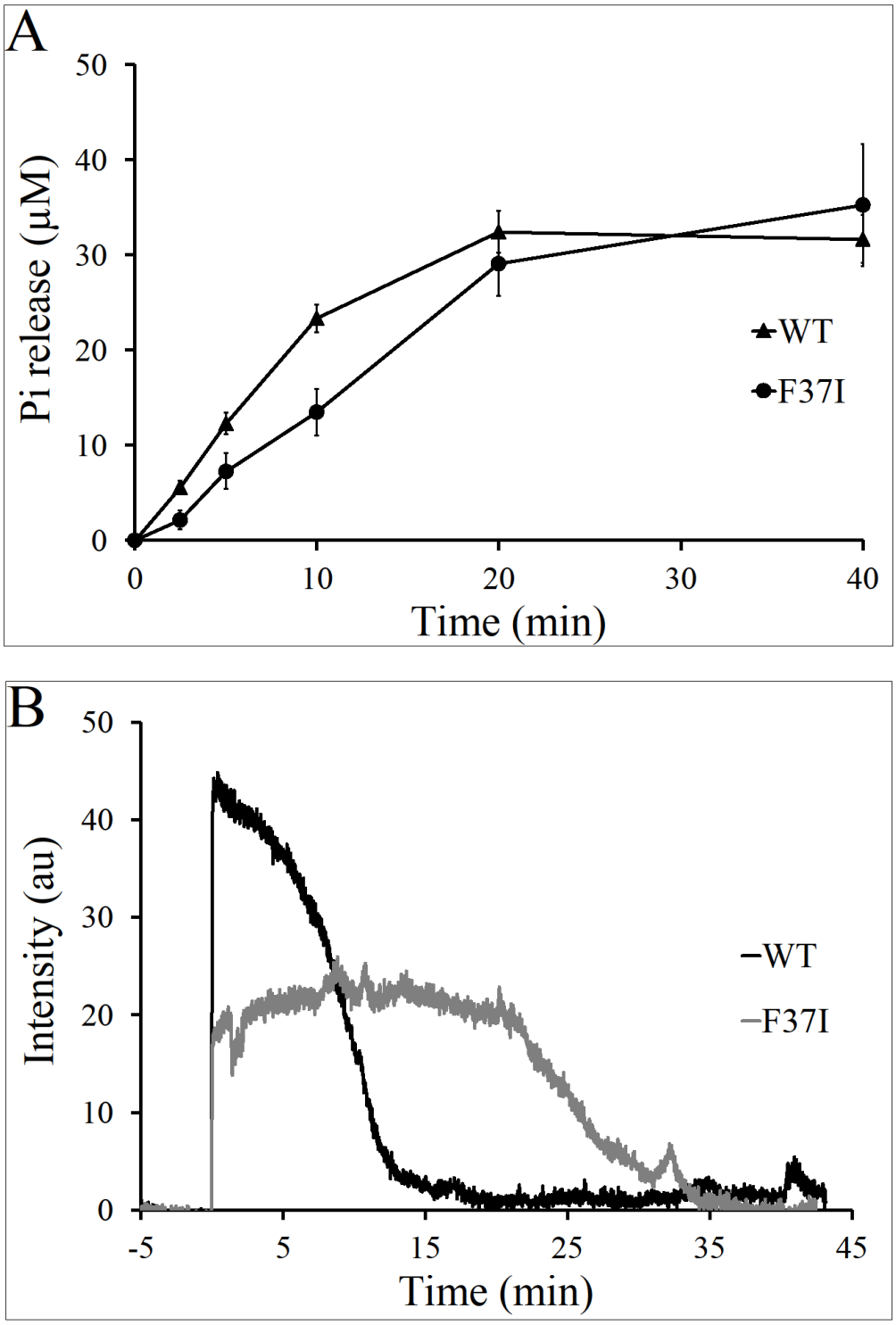

Figure S9. Biochemical analyses of *S. coelicolor* FtsZ and FtsZ(F37I). Representative results of GTPase assays **(A)** and right-angle light scattering assays of polymer formation **(B)** of the F37I mutant proteins compared to wild-type FtsZ protein. GTPase assays were performed in three independent experiments (n = 3) with each in duplicate and the error bars show the standard deviation in each data set. Experiments were conducted at 3.5 µM FtsZ and 50 µM GTP in MMK buffer pH 6.5 at 30°C.

Movie S1: Time-lapse fluorescence microscopy of wild-type FtsZ in sporulating *S. venezuelae*. The movie consists of fluorescence images of FtsZ-YPet (left) and the corresponding phase-contrast images (right) of strain LUV052 (*ftsZ*$^+$ *attB*$_{\phi BT1}$*::*pKF543[*ftsZ-ypet*]). The cells were cultivated in CellASIC ONIX microfluidic plates (Merck). After an initial period of vegetative growth, sporulation was stimulated by switching to spent medium obtained from a sporulating liquid culture of the *S. venezuelae* wild-type strain. Time interval between frames is 30 min. Scale bar, 5 μm

Movie S2: Time-lapse fluorescence microscopy of mutant FtsZ(F37I) in sporulating *S. venezuelae*. The movie consists of fluorescence images of FtsZ(F37I)-YPet (left) and the corresponding phase-contrast images (right) of strain LUV057 (*ftsZ*(F37I) *attB*$_{\phi BT1}$*::*pKF544[*ftsZ*(F37I)-*ypet*]). The cells were cultivated in CellASIC ONIX microfluidic plates (Merck). After an initial period of vegetative growth, sporulation was stimulated by switching to spent medium obtained from a sporulating liquid culture of the *S. venezuelae* wild-type strain. Time interval between frames is 30 min. Scale bar, 5 μm

Supplementary references

Bush, M.J., Chandra, G., Al-Bassam, M.M., Findlay, K.C., and Buttner, M.J. (2019) BldC delays entry into development to produce a sustained period of vegetative growth in *Streptomyces venezuelae*. *MBio* **10**.

Di Tommaso, P., Moretti, S., Xenarios, I., Orobitg, M., Montanyola, A., Chang, J.M., Taly, J.F., and Notredame, C. (2011) T-Coffee: a web server for the multiple sequence alignment of protein and RNA sequences using structural information and homology extension. *Nucleic Acids Res.* **39**: W13-17.

Donczew, M., Mackiewicz, P., Wrobel, A., Flärdh, K., Zakrzewska-Czerwinska, J., and Jakimowicz, D. (2016) ParA and ParB coordinate chromosome segregation with cell elongation and division during *Streptomyces* sporulation. *Open Biol* **6**: 150263.

Flärdh, K., Leibovitz, E., Buttner, M.J., and Chater, K.F. (2000) Generation of a non-sporulating strain of *Streptomyces coelicolor* A3(2) by the manipulation of a developmentally controlled *ftsZ* promoter. *Mol. Microbiol.* **38**: 737-749.

Gregory, M.A., Till, R., and Smith, M.C. (2003) Integration site for *Streptomyces* phage phiBT1 and development of site-specific integrating vectors. *J. Bacteriol.* **185**: 5320-5323.

Hanahan, D. (1983) Studies on transformation of *Escherichia coli* with plasmids. *J. Mol. Biol.* **166**: 557-580.

Kieser, T., Bibb, M.J., Buttner, M.J., Chater, K.F., and Hopwood, D.A., (2000) *Practical Streptomyces Genetics*. The John Innes Foundation, Norwich, UK.

McCormick, J.R., Su, E.P., Driks, A., and Losick, R. (1994) Growth and viability of *Streptomyces coelicolor* mutant for the cell division gene *ftsZ*. *Mol. Microbiol.* **14**: 243-254.

Robert, X., and Gouet, P. (2014) Deciphering key features in protein structures with the new ENDscript server. *Nucleic Acids Res.* **42**: W320-324.

Schlimpert, S., Wasserstrom, S., Chandra, G., Bibb, M.J., Findlay, K.C., Flärdh, K., and Buttner, M.J. (2017) Two dynamin-like proteins stabilize FtsZ rings during *Streptomyces* sporulation. *Proc. Natl. Acad. Sci. USA* **114**: E6176-E6183.

Wasserstrom, S., Grantcharova, N., Ubhayasekera, W., Ausmees, N., Sandblad, L., and Flärdh, K. (2013) Non-sporulating *ftsZ* mutants in *Streptomyces coelicolor* reveal amino acid residues critical for FtsZ polymerization dynamics. *Microbiology* **159**: 890-901.